

Discovery of Nuclear X-ray Sources in SINGS Galaxies

C. J. Grier¹, S. Mathur¹, H. Ghosh², L. Ferrarese³

ABSTRACT

We present the results of a search for nuclear X-ray activity in nearby galaxies using *Chandra* archival data in a sample of 62 galaxies from the *Spitzer* Infrared Nearby Galaxy Survey (SINGS). We detect 37 nuclear X-ray sources; seven of these are new detections. Most of the nuclear X-ray sources are likely to be AGNs. The fraction of galaxies hosting AGNs is thus about 60%, much higher than that found with optical searches, and demonstrates the efficacy of X-ray observations to find hidden AGNs in optically normal galaxies. We find that the nuclear X-ray sources are preferentially present in earlier type galaxies. Unlike what is observed at high redshift for high-luminosity AGNs, we do not find a strong correlation between the AGN luminosity and the $24\mu\text{m}$ luminosity of the host galaxy; we find a strong correlation with the $3.6\mu\text{m}$ luminosity instead. This suggests that at the present epoch the accretion rate depends on the total mass of the galaxy, as perhaps does the black hole mass.

Subject headings: galaxies: active — galaxies: nuclei — X-rays: galaxies

1. INTRODUCTION

The past decade has seen extraordinary growth in our understanding of supermassive black holes (SMBHs), with secure detections, mass measurements and new demographic information (see Ferrarese & Ford 2005 and references therein; FF05 hereafter). Knowledge of the mass function of SMBHs directly affects our understanding of SMBH formation and growth, nuclear activity, and the relation of SMBHs to the formation and evolution of galaxies in hierarchical cold dark matter models (e.g. Menci et al. 2004). The cumulative mass function needed to explain the energetics of high redshift quasars implies that all galaxies in

¹Department of Astronomy, The Ohio State University, 140 W 18th Ave, Columbus, OH 43210; grier@astronomy.ohio-state.edu

²CNRS/CEA-Saclay, 91911 Gif-sur-Yvette, France

³Hertzberg Institute of Astrophysics, 5071 West Saanich Road, Victoria, BC, V9E 2E7, Canada

the local universe should host a SMBH (e.g. Marconi et al. 2004, Shankar et al. 2004), but we do not know whether this is indeed the case.

Many SMBHs have been found, and their masses measured through stellar and gas dynamics methods at the high end of the SMBH mass function (FF05). In the intermediate mass range, around $10^8 M_\odot$, we know of the existence of SMBHs as active galactic nuclei (AGNs); their masses are measured through reverberation mapping or using scaling relations with emission line widths and luminosity (e.g. Blandford & McKee 1982, Peterson 1993, Wandel et al. 1999, Kaspi et al. 2000, 2005). When considering smaller SMBHs or galaxies farther away, mass measurement is more difficult; the sphere of influence of the black hole in these objects is too small to resolve, so we cannot use dynamical estimates, and if we do not see AGN activity at visible wavelengths, we cannot use reverberation mapping. For these reasons, the low-mass end of the SMBH mass function is largely unexplored; indeed we still do not know whether all galaxies host SMBHs.

Because of these difficulties, we turn to AGN signatures to help us probe the existence of low-mass SMBHs. The observed “downsizing” of AGNs (e.g. Hasinger et al. 2005), in which more luminous AGNs are seen to be accreting more actively at higher redshifts and less luminous objects are expected to dominate in the local universe, implies that proportionally more low-mass SMBHs should still be accreting at present. The low mass SMBHs are expected to be present in late-type galaxies. It is possible that the nearby “normal” galaxies appear “normal” because AGN activity is weak and is washed out by starlight when viewed in the optical bands. However, if these objects are in fact accreting, we should observe many of them in X-ray emission. X-rays are well-suited to identifying low-mass systems in late-type galaxies because they can penetrate obscuring material, which in many cases can mask out the emission-line regions surrounding the AGN. Additionally, for low luminosity AGNs the optical light can be overwhelmed by the host galaxy light; X-rays, once again, are helpful in this respect because galaxies themselves are not very bright in X-rays. Indeed, there have been several successful efforts using X-rays to identify AGN activity in galaxies residing in clusters (Martini et al. 2002) and in fields (Brand et al. 2005).

In an effort to improve our knowledge of the low-mass end of the SMBH mass function, we conducted a search for low-luminosity AGN candidates using *Chandra* (Ghosh et al. 2008, 2009, 2010a, 2010b). Our program was successful in that we discovered AGNs in what were thought to be normal galaxies. Through extensive spectral, timing and multiwavelength analysis we classified nuclear X-ray sources in 56 galaxies and found 17 that are almost certainly AGN. Thus at least 30% of normal galaxies are actually active. The inferred luminosities of these sources range from $10^{37.5}$ to 10^{42} erg s $^{-1}$. In a few objects where SMBH masses were known from stellar/gas dynamics methods, we find accretion rates as low as

10^{-5} of the Eddington limit.

We found that AGNs are present in galaxies of all Hubble types. The distribution of luminosities in a given type and across Hubble types is wide. Moreover, in a given Hubble type, some galaxies host AGNs (down to our flux limit), but some do not. Thus the important outstanding question is: What governs accretion onto a SMBH? At low redshift, the merger rate is low, so the accretion is unlikely to be merger driven. Is it related to star formation rate, as seen at high redshift (e.g. Netzer 2009a, Lutz et al. 2008)? Is it the galactic structure in the central regions, such as bars or nuclear spirals (Pogge & Martini 2002)? Multiwavelength data are necessary to answer these fundamental questions and the *Spitzer* Infrared Nearby Galaxy Survey (SINGS) provides such data. Most SINGS galaxies have been observed with *Chandra*, so we searched for nuclear X-ray sources in these galaxies. The main goals of this study were to investigate in detail the X-ray properties of the SINGS sample, detect potential new low-luminosity nuclear activity, and investigate possible connections between nuclear X-ray luminosity and various multiwavelength properties of the host galaxies.

2. DATA AND ANALYSIS

2.1. Galaxy Sample

Our galaxy sample consists of objects from SINGS and is described in detail in Kennicutt et al. (2003). The original sample contained 75 galaxies within 30 Mpc that were chosen to obtain a broad range of galaxy properties to represent the composition of the local universe. This sample was well-suited for our study because these galaxies have been the subjects of many different investigations at many different wavelengths, and we hoped to investigate various properties of galaxies and their connection to the nuclear X-ray activity. Basic information on each of the galaxies in our sample was retrieved from Kennicutt et al. (2003) and presented in Table 1 along with information on the *Chandra* observations used. There were 13 objects in the SINGS sample for which data was unavailable in the *Chandra* archive; the remaining 62 SINGS galaxies had been observed with *Chandra* by the time of this study and the data are available for public use. These 62 galaxies constitute the sample in our study. The SINGS sample is composed of both quiescent and active galaxies; our X-ray sample includes 13 objects whose nuclei are optically identified as Seyferts, nine that are identified as H II regions, 11 that contain low ionization nuclear emission regions (LINERs), and seven that are optically identified as starbursts. The remaining 22 galaxies in our study had no listed optical nuclear classifications.

2.2. Data Analysis

We used the *Chandra* Interactive Analysis of Observations software (CIAO)¹ v3.4 to process images and extract source counts (Fruscione et al. 2006). X-ray data were downloaded from the *Chandra* archive and filtered to exclude background flares, following the procedure of Ghosh et al. (2008). We used the CIAO task *wavdetect* to determine the positions of the sources. We then searched for nuclear sources using object positions listed in the NASA/IPAC Extragalactic Database (NED). *Chandra*’s 90% source location error circle has a radius of less than 0".6 and less than 1% of sources fall outside a 1" radius. Therefore, sources that were detected within a 1" radius of the listed position in NED are considered nuclear detections.

Source counts were extracted from a region centered on the source found by *wavdetect*; the radius of the source region is equal to the 95% encircled-energy radius or 2".3 (4.67 pixels), whichever is greater. We extracted the background counts from an annulus with an outer radius of 5 times the radius of the source region and an inner radius of twice the radius of the source region. Any other source that fell inside this annulus was excised from the image before counts were extracted. Broadband source counts were extracted in the 0.3-8.0 keV range; counts were also extracted in the 0.3-2.5 keV (soft) and the 2.5-8.0 keV (hard) bands. We also calculated the hardness ratios, defined as $HR = (H - S)/(H + S)$, where H represents the number of hard counts and S represents soft counts, when possible.

We retrieved *Spitzer* IRAC, MIPS, and 2MASS fluxes from Dale et al. (2007), which are measured from image mosaics that are large enough to detect emission out to R_{25} in each galaxy. These flux densities therefore represent the total fluxes of the galaxy at a given wavelength. We also searched for 2MASS point source detections at the positions of the nuclei in these galaxies; all of our detected X-ray sources have 2MASS counterparts that are listed in the 2MASS point source catalog (Skrutskie et al. 2006). The 2MASS magnitudes are measured using a PSF profile-fitting algorithm (see catalog for details) within an aperture of $\sim 4''$ centered on the position of the detected source. We also obtained 1.4 GHz integrated flux densities for those sources that were detected in the VLA “Faint Images of the Radio Sky at Twenty-Centimeters” survey (FIRST; White et al. 1997). The FIRST survey has a resolution of about 5"; fluxes were measured by fitting a Gaussian to the observations. To summarize, the X-ray, 2MASS source, and FIRST luminosities are nuclear luminosities, while the *Spitzer* and 2MASS global luminosities from Dale et al. (2007) include light from the entire galaxy.

¹<http://cxc.harvard.edu/ciao3.4/index.html>

3. X-RAY RESULTS

3.1. New Detections

We detected nuclear sources in 37 objects in this sample. Six of these detections are in galaxies that have not yet been examined for nuclear X-ray activity using *Chandra* observations. We also report a new detection in one galaxy (NGC 855) that has been previously searched but its nucleus had not been detected. We discuss the new detections individually below. All quoted X-ray luminosities are calculated using a power law with $\Gamma = 2$ and Galactic absorption.

In order to quantify our assumptions for AGN activity, we computed IR to X-ray slopes in these new objects to see how they compared with observed slopes in known AGNs. We compare our measured slopes with Laor et al. (1994), who measure the average IR to soft X-ray slope $\langle \alpha_{\text{irs}} \rangle = -1.26 \pm 0.11$ in their sample of quasars, defining α_{irs} as

$$\alpha_{\text{irs}} = \log(f_{0.3\text{keV}}/f_{1.69\mu\text{m}})/2.611. \quad (1)$$

We estimate α_{irs} for the seven objects discussed individually below. We calculate $f_{0.3\text{keV}}$ by using a $\Gamma = 2$ power law and our observed integrated 0.3–8 keV fluxes to estimate the flux at 0.3 keV. As mentioned, we have 3.6 μm fluxes for all of these objects from Dale et al. (2007), which we use to approximate $f_{1.69\mu\text{m}}$. Spectral templates from Assef et al. (2010) show that for a typical AGN, the difference in flux between 1.69 μm and 3.6 μm is about a factor of 1/3. We correct our fluxes by this factor, which translates to an increase in α_{irs} in our sources of 0.18. Typical uncertainties in α_{irs} for these 7 measurements are around 0.2. We can then directly compare our slopes with the results of Laor et al; individual measurements are discussed below.

3.1.1. NGC 1404

NGC 1404 is a type E1 galaxy at a distance of 25.1 Mpc. There was no previously listed nuclear classification for this object. There are several publications investigating NGC 1404 in X-rays but to our knowledge, none of them examine the nuclear X-ray properties of the galaxy. We have four observations of NGC 1404 and it was detected in all four; we here report on only the longest observation. NGC 1404 was observed by *Chandra* using the ACIS-I camera for ~ 44 ks and detected with 797 net broadband counts. Its hardness ratio $\text{HR} = -0.904$. We estimate $L_{0.3-8\text{keV}} = 1.55 \times 10^{40} \text{ erg s}^{-1}$ for this source. This point source was detected in the 2MASS survey with $L_J = 7.6 \times 10^{43} \text{ erg s}^{-1}$, $L_H = 1.4 \times 10^{44} \text{ erg s}^{-1}$, and $L_K = 2.9 \times 10^{44} \text{ erg s}^{-1}$. Given the 2MASS luminosities, the bolometric luminosity of the

source is high enough for it to be an AGN. We measure $\alpha_{\text{irs}} = -1.35$; this slope is consistent with that expected of an AGN as measured by Laor et al. (1994). Based on the *Chandra* image (Figure 1), there is a potential for extended emission as well, which could originate from the circumnuclear region, as observed in Seyfert 2 galaxies (Ghosh et al. 2007).

3.1.2. NGC 2798

This is an SBa galaxy at a distance of 24.7 Mpc that was observed for ~ 5 ks. Its nucleus was listed by Kennicutt et al. (2003) and references therein as a starburst region based on optical spectroscopy. We detect the nucleus with 73 counts; the nuclear source is shown in Figure 1. Its hardness ratio is $\text{HR} = -0.82$ and we estimate $L_{0.3-8\text{keV}} = 7 \times 10^{39} \text{ erg s}^{-1}$. The nucleus was detected by 2MASS with observed $L_J = 4.8 \times 10^{43} \text{ erg s}^{-1}$, $L_H = 1.1 \times 10^{44} \text{ erg s}^{-1}$, and $L_K = 1.7 \times 10^{44} \text{ erg s}^{-1}$. This source is also detected in FIRST with an integrated 1.4GHz flux density of 61.38 mJy. We measure $\alpha_{\text{irs}} = -1.16$, again consistent with the slope expected in AGNs. Because this nuclear source is also an X-ray and radio source and has such high 2MASS luminosities, we identify it here as an AGN, though there is likely a starburst contribution to the X-ray flux.

3.1.3. NGC 2976

This SAc galaxy is at a distance of 3.5 Mpc, and its nucleus is listed as an H II region in Kennicutt et al. (2003). It was observed for ~ 10 ks and the nucleus was detected with 6 broadband counts. The source is shown in Figure 1. There are insufficient counts to recover a spectrum and HR, but we estimate $L_{0.3-8\text{keV}} = 6.2 \times 10^{36} \text{ erg s}^{-1}$, again using a standard power law model. The nucleus was detected by 2MASS with $L_J = 3.5 \times 10^{40} \text{ erg s}^{-1}$, $L_H = 7.6 \times 10^{40} \text{ erg s}^{-1}$, and $L_K = 1.0 \times 10^{41} \text{ erg s}^{-1}$. The 2MASS luminosities of this source are not as high as the two galaxies listed above, but the K -band luminosity is high enough that the source is unlikely to be an X-ray binary. We measure $\alpha_{\text{irs}} = -1.9$, which is somewhat steeper than expected, but is consistent with an AGN with an obscured X-ray source.

3.1.4. NGC 3198

NGC 3198 is an SBc galaxy at a distance of 9.8 Mpc. It was observed by *Chandra* for 61.8 ks and was detected with 108 broadband counts, corresponding to $\log L_{0.3-8\text{keV}} = 1.4 \times 10^{38} \text{ erg s}^{-1}$. The source is shown in Figure 1. The X-ray hardness ratio $\text{HR} = -0.535$. The

nucleus was detected by 2MASS with $L_J = 1.2 \times 10^{42}$ erg s $^{-1}$, $L_H = 2.4 \times 10^{42}$ erg s $^{-1}$, and $L_K = 4.0 \times 10^{42}$ erg s $^{-1}$. The nucleus is identified in the FIRST survey with an integrated flux density of 1.89 mJy. We measure $\alpha_{\text{irs}} = -1.65$, which is again consistent with the presence of an AGN with an obscured central X-ray source. As in the case of NGC 2798 above, this is highly likely to be an AGN based on its 2MASS luminosities and the fact that it is both an X-ray and radio source.

3.1.5. Mrk 33

Mrk 33 is categorized as an irregular galaxy in NED but is listed by SIMBAD as a pair of interacting galaxies at a distance of 21.7 Mpc. Its nucleus is also listed as a starburst region by Kennicutt et al. (2003). The nucleus was detected with two separate components. One source is detected in both the soft and hard bands, but the other source disappears completely in the hard band. Here we focus only on the hard source; while a soft-only source could be an AGN if it is completely obscured and all we see is reprocessed/starburst emission, we cannot be sure without a good quality spectrum. Because the 95% energy radii of the two sources overlap, we were unable to disentangle the two sources completely. Since the counts in the soft band are similar in each source, we extracted counts from a region encircling both sources and halved the number of soft counts to obtain counts for the hard source. We attribute all of the hard counts to the hard source. Our X-ray image is shown in Figure 1. The harder source is detected with 100 broadband counts, corresponding to a luminosity $L_{0.3-8\text{keV}} = 2.2 \times 10^{39}$ erg s $^{-1}$. The hardness ratio is $\text{HR} = -0.640$. The hard source was detected by 2MASS with $L_J = 1.3 \times 10^{43}$ erg s $^{-1}$, $L_H = 2.2 \times 10^{43}$ erg s $^{-1}$, and $L_K = 2.8 \times 10^{43}$ erg s $^{-1}$. It is also a radio source, detected in the FIRST survey with an integrated flux density of 9.56 mJy. Again, its high 2MASS luminosities and that it is both an X-ray and a radio source merit its inclusion as an AGN candidate. Furthermore, we measure $\alpha_{\text{irs}} = -1.08$ in this source, again is consistent with our expectations in AGNs. As noted above, we cannot be sure that the soft source is an AGN. However, it is reasonable to suspect that it too is an obscured AGN at the center of the second galaxy of the pair. Much follow up is required on this particular object to determine if this is in fact the case.

3.1.6. NGC 4450

NGC 4450 is an Sab galaxy at a distance of 20 Mpc and its nucleus has been optically identified as a LINER. It was observed by *Chandra* for 3.7 ks and detected with 223 counts. We estimate $L_{0.3-8\text{keV}} = 5.0 \times 10^{40}$ erg s $^{-1}$ and hardness ratio $\text{HR} = -0.695$. The source

is shown in Figure 1. Its nucleus was detected by 2MASS with $L_J = 3.8 \times 10^{43} \text{ erg s}^{-1}$, $L_H = 7.6 \times 10^{43} \text{ erg s}^{-1}$, and $L_K = 8.1 \times 10^{43} \text{ erg s}^{-1}$. We measure $\alpha_{\text{irs}} = -1.04$ in this source, which again is consistent with expectations in AGNs to within our uncertainties. It is also a radio source detected by FIRST with an integrated flux density of 6.53 mJy, and is clearly an AGN.

3.1.7. NGC 855

There has been some disagreement regarding the morphological classification of NGC 855. While this object is listed as an elliptical, many authors in fact argue that this is a dwarf elliptical galaxy. We discuss its classification further in section 5. We have one 59.48 ks observation of the NGC 855 and detect the nucleus with 108 broad band counts. Zhang et al. (2009) used a 1.7 ks exposure of this object and did not detect the source— this makes our detection a new detection. The nuclear source is shown in Figure 1. We estimate $L_{0.3-8\text{keV}} = 1.6 \times 10^{38} \text{ erg s}^{-1}$. The nucleus was also detected by 2MASS with $L_J = 1.5 \times 10^{42} \text{ erg s}^{-1}$, $L_H = 1.5 \times 10^{42} \text{ erg s}^{-1}$, and $L_K = 1.9 \times 10^{42} \text{ erg s}^{-1}$. We measure $\alpha_{\text{irs}} = -1.35$ in this source, which again is consistent with expectations in AGNs; this object is very likely an AGN.

3.2. Detections in objects with previous publications

There were 44 objects on which previous analysis has been done; previous publications that investigate the nuclei of these galaxies using *Chandra* observations are listed in Table 1. We analyzed these as well to provide a consistent analysis of the entire sample. Our measurements are presented in Tables 2 and 3. With the exception of NGC 4826, all of our results are consistent with previous measurements. Our measurements for this object are presented below. In the cases of NGC 3521, NGC 3627, NGC 4569, NGC 4594, and NGC 4725, we have analyzed data with longer exposure times than have previously been published.

3.2.1. NGC 4826

NGC 4826 is an SAab galaxy that is optically identified as a Seyfert 2 (Véron-Cetty & Véron 2006). We detect a point source here, while neither Ho et al. (2001) or Zhang et al. (2009) report a nuclear point source detection. Figure 1 shows our *Chandra* image. The detected

source is soft, and therefore unlikely to be direct AGN emission. However, this could be an obscured AGN in which only circumnuclear emission is visible, as is often the case with Seyfert 2 galaxies (Ghosh et al. 2007).

3.3. Non-detections

We do not detect a nuclear source in 25 of the galaxies in our sample. Several of these objects are irregular galaxies; for these objects we searched for X-ray sources within a few arcseconds of the galaxy position as listed on NED, since in these cases the “center” of the galaxy is poorly defined. 3σ upper limits to all non-detections are given in Table 2; the upper limits were calculated by extracting source counts within a $2''.3$ radius circle centered on the nuclear position as listed on NED and background counts from an annulus with the same measurements as the background regions for the detected sources. In all cases, our results are consistent with previous results. In the cases of Ho IX, NGC 4625, NGC 4826, and NGC 5474, we used data with longer exposure times than previous studies, but we still do not detect the nuclei in these sources.

3.4. *Chandra* Results: Summary

Altogether, out of the 75 SINGS galaxies, 62 have data in the *Chandra* archive and we detect nuclear X-ray sources in 37 of them. The nuclear X-ray sources, however, could be stars, binaries, supernova remnants or AGNs. In the Ghost et al. papers (§1) we did extensive spectral, timing and multiwavelength analysis to identify the nuclear X-ray sources. Similarly, we show that the new detections in SINGS galaxies listed above are highly likely to be AGNs by examining their properties in multiple wavelengths as well as comparing their IR to X-ray slopes with those of identified AGNs. As discussed in Ghosh et al. (2010a), when the sample as a whole is considered it becomes statistically unlikely that all detected nuclear X-ray sources are contaminants which happen to be at the center of the galaxy (see also Ho 2009, Zhang et al. 2009). We therefore argue that statistically, most, if not all, of the nuclear X-ray sources in SINGS galaxies are AGNs; we assume them to be AGNs for the rest of this paper.

4. MULTIWAVELENGTH ANALYSIS

4.1. *Spitzer* Measurements

As mentioned above, we obtained *Spitzer* IRAC and MIPS flux densities from Dale et al. (2007) to see how the X-ray activity is related to other galaxy properties. We converted these flux densities to observed luminosities; since these objects are all at very low redshift, this did not require a K-correction. Figure 2 shows the *Spitzer* luminosities of the galaxies plotted against the nuclear (i.e. AGN) X-ray luminosities from this study. We observe correlations between the nuclear X-ray luminosity and mid-infrared luminosity at all wavelengths, but the correlation is the strongest at 3.6, 4.5 and 5.8 μm . The measured ratios and intercepts for all of the correlations observed are given in Table 4. We also compute the Spearman and Pearson’s coefficients in each case to determine the strength of the correlation. In both cases, a coefficient of 1 represents a perfect linear correlation between the two parameters, a coefficient of 0 represents no correlation, and negative coefficients show a correlation in the opposite direction. The coefficients are presented in Table 4. We also calculated the probability that the the observed correlation is not real, $P(r)$. The correlations between nuclear X-ray luminosity and infrared luminosities at 3.6, 4.5, and 5.8 μm are significant at greater than 99.9%; the correlation at 8 μm is significant to 99%, and those at 24, 70, and 160 μm , while much weaker than the other correlations, are still correlated at $\sim 90\%$ certainty. To ensure that the observed correlations are not artifacts of sample selection or flux limits, we have also included upper limits of *Chandra* non-detections in Figure 2. It is clear that the observed correlations are robust.

Note that our *Spitzer* flux measurements measure the *global* infrared fluxes– not just the nuclear fluxes– so comparing 3.6 μm and nuclear X-ray luminosity does not simply compare AGN luminosities in two different bands unless the nuclear infrared flux completely dominates the infrared flux of the entire galaxy. To be sure that the nuclei of these galaxies were not dominating the global flux in the infrared, we obtained nuclear surface brightness estimates from Muñoz-Mateos et al. (2009), which allowed us to estimate the total flux within a 6'' radius of the nucleus of each galaxy. We then subtracted this flux from the global IR flux to see how much the total was affected by removing the nuclear component, and in nearly all cases, the removal of the nuclear IR flux did not have a significant effect. This indicates that our global infrared fluxes do in fact represent the flux of the galaxy rather than the AGN. Light at these wavelengths is mostly contributed by stars; the observed correlation between nuclear X-ray luminosity and IR luminosity is therefore a manifestation of an observed relation between AGN luminosity and host galaxy mass. The relationship between M_{BH} and stellar mass in the host bulge has been well-established (e.g. Kormendy & Richstone 1995, Magorrian et al. 1998, Bentz et al. 2009), as has the relationship between the size of the host

bulge and the total stellar mass in the galaxy (Ferrarese 2002, Baes et al. 2003). Therefore it would follow that M_{BH} correlates with the host galaxy stellar mass. Our observed correlation between X-ray luminosity and host galaxy stellar mass suggests that accretion rate (\dot{M}) also depends on the host galaxy mass; this is a surprising new discovery.

4.2. 2MASS J , H , and K band Measurements

We looked for potential relations between nuclear 2MASS luminosities and nuclear X-ray luminosities. As demonstrated in Figure 3, we observe trends with nuclear X-ray luminosity that are well-fit by power laws; the best-fit parameters and correlation coefficients are again given in Table 4. The correlation coefficients indicate that the correlations are significant in all three 2MASS bandpasses shown. Such correlations should exist between X-ray and IR luminosities of AGNs; observations of these correlations further support the identification of nuclear X-ray sources as AGNs. The scatter around the correlations and the non-unity slopes also suggest varying amounts of obscuration, dust or intrinsic variations in the SED.

We also obtained global J , H , and K -band fluxes from Dale et al. (2007). On a global scale, K band magnitudes are good stellar mass indicators, so we looked to see if there was a correlation between nuclear X-ray luminosity and global K band luminosity. Figure 4 shows this correlation; while shallower than the $L_{K,\text{nuc}}/L_X$ relation, it is still a rather strong correlation. As with the *Spitzer* data, we checked to be sure that the K band emission is not dominated by the nuclei, and in most cases it did not. We removed the galaxies in which the nuclear K band flux was greater than 50% of the total flux and determined that these objects did not affect the measured correlation.

In addition, we examined the 1.4 GHz fluxes from the FIRST survey (Figure 5) and observe no correlation between the nuclear X-ray flux and the integrated radio flux.

4.3. Star Formation Rates

Several studies in recent years have investigated a possible connection between star formation and AGN luminosity in active galaxies and quasars (e.g. Netzer 2009a, Lutz et al. 2008). These correlations have been measured primarily using star formation rate (SFR) indicators in the FIR, $\text{H}\alpha$ and O II fluxes, or features that arise from polycyclic aromatic hydrocarbons (PAHs) that are measured in the mid-infrared. Netzer (2009b) and Lutz et al. (2008) both measure slopes of around 0.8 when comparing the bolometric AGN luminosity (using either L_{5100} or $[\text{O I}/\text{O II}]$ to estimate L_{bol}) to 60 μm luminosity. While we do not have

the same observables, we can check whether the galaxies in our sample show a correlation between AGN X-ray luminosity and the $70\ \mu\text{m}$ luminosity. We find a slope of ~ 0.2 when comparing $L_{0.3-8\text{keV}}$ to $L_{70\mu\text{m}}$. Since the AGNs are likely to be obscured, perhaps the X-ray luminosity is not a perfect indicator of the total AGN luminosity; the broad correlation between $L_{K,\text{nuc}}$ and $L_{0.3-8\text{keV}}$ mentioned above, however, suggests that this is not a bad assumption. A comparison between nuclear K-band luminosity $L_{K,\text{nuc}}$ and global $L_{70\mu\text{m}}$ results in a slope of 0.2 (see Figure 6). Similarly shallow slopes are observed for correlations between $L_{0.3-8\text{keV}}$ and other FIR measurements (Table 4). Thus, regardless of whether we use X-ray, K-band, or other IR luminosities as indicators of AGN activity, we do not see a strong correlation of AGN activity with star formation activity as seen at higher redshifts.

We also examined the SFRs in our sample of nuclear X-ray detected galaxies using SFRs computed by Calzetti et al. (2010). The SFRs were calculated using the $24\ \mu\text{m}$ luminosity combined with the $\text{H}\alpha$ luminosity as a composite star formation rate indicator; see Calzetti et al. (2010) for details in these calculations. Figure 7 shows the star formation rate per unit area in our sample. We observe no significant correlation between nuclear X-ray luminosity and SFR, which again is no surprise, as we do not observe a strong correlation between $L_{0.3-8\text{keV}}$ and $L_{24\mu\text{m}}$ and therefore do not expect SFRs that are calculated using $L_{24\mu\text{m}}$ to correlate either. Total SFR (rather than SFR per unit area) was also examined and shows no significant correlation with $L_{0.3-8\text{keV}}$.

5. DISCUSSION

In a sample of 62 SINGS galaxies with available *Chandra* archival data, we detect 37 nuclear X-ray sources. Eleven detections are in objects whose nuclei have been identified as LINERs, five detections are in identified H II regions, twelve are in galaxies hosting Seyfert nuclei, and two occurred in starburst galaxies. The other seven detections were in galaxies which do not have a previous nuclear classification. We argue that most of these 37 detections are likely low-luminosity AGNs. We present nuclear X-ray fluxes, luminosities, and hardness ratios for all of these sources. We look for connections between infrared and X-ray luminosities and observe a correlation between nuclear X-ray luminosity and various IR luminosities, including IRAC $3.6\ \mu\text{m}$ and $4.5\ \mu\text{m}$ bands and 2MASS J , H , and K bands. Unlike the results for higher redshift AGNs, we find that the AGN activity is *not* strongly correlated with the star formation activity, though a mild trend is observed. We find instead a strong correlation with the stellar mass of a galaxy. As discussed above, it is well known that the mass of the nuclear BH is correlated with the bulge mass or perhaps the total galaxy mass. Our observations suggest that even the accretion rate depends on the galaxy mass.

It is possible that all of the galaxies are emitting at a similar fraction of their Eddington luminosity; galaxies with higher mass BHs would then be more luminous. New observations with *Herschel* (Shao et al. 2010) also show that the correlation between AGN activity and star formation activity disappears at lower AGN luminosity even at higher redshift. It thus appears that the AGN-SFR correlation is not as generic a phenomenon as once thought.

Figure 8 shows the distribution of Hubble types among the SINGS galaxy sample in our study. We show the number of galaxies at each Hubble type T and compare this with the number of galaxies with nuclear X-ray detections at each T type. We observe nuclear X-ray activity in nearly all of the galaxies towards the early end of the Hubble sequence, and report no detections in Sdm and Sm galaxies and only two nuclear X-ray detections in irregular or peculiar galaxies. We may expect such a result if the bulge-less galaxies do not harbor a nuclear BH. However, this is unlikely to be the case, as BHs in bulge-less galaxies have been detected through optical (Peterson et al. 2005; Shields et al. 2008), IR (Satyapal et al. 2007, 2009) and X-ray (Ghosh et al. 2008) studies. Once again, it may suggest lower accretion rates.

We also show the $3.6\ \mu\text{m}$ luminosity of SINGS galaxies as a function of Hubble Type in Figure 9. As one would expect, earlier-type galaxies show a higher $3.6\ \mu\text{m}$ luminosity than later-type galaxies, reflecting the differences in stellar mass between early and late-type galaxies. Figure 9 shows that NGC 855 is a significant outlier on the relation. We re-checked the classification of the source and found that there is some disagreement between sources over what type of galaxy this is. While it is listed in the RC3 catalog as an elliptical (de Vaucouleurs et al. 1991), other sources suggest that this galaxy is actually a dwarf elliptical (e.g. Roussel et al. 2007) or even a late-type spiral (Phillips et al. 1996). Our observed correlation supports the reclassification of NGC 855 as a dwarf elliptical.

Given the anticorrelation of $3.6\mu\text{m}$ luminosity with the Hubble type and the correlation between $3.6\mu\text{m}$ luminosity with X-ray luminosity, we expect to see an anticorrelation between the X-ray luminosity and the Hubble type. However, as shown in Figure 10, there appears to be no correlation between these measurements. This is likely because for every Hubble type there is a wide range of $3.6\mu\text{m}$ luminosities and also a wide range of X-ray luminosities. We do notice that none of the galaxies later than $T = 5$ have particularly high $L_{0.3-8\text{keV}}$.

6. CONCLUSION

We find that about 60% of SINGS galaxies host nuclear X-ray sources which are likely to be AGNs. This fraction is much larger than that found through optical studies (e.g.

Ho et al. 1997) and shows the efficacy of X-ray observations to find hidden AGNs in normal galaxies. We find that for our sample of galaxies AGN activity is correlated with the stellar mass of the galaxy. This is a surprising new result and suggests that together with the mass of the SMBH, accretion rate also depends on galaxy mass. Unlike the merger driven black hole growth observed at high redshift for high-luminosity AGN, there appears to be an alternative mode of black hole growth at the present epoch in late type galaxies. It has been suggested in literature that the total mass of a galaxy, not just the bulge mass, is the primary driver of the mass of the SMBH (Ferrarese 2002, Baes et al. 2003); our results support such a scenario.

We are grateful to the SINGS team for the multiwavelength survey of nearby galaxies. This publication makes use of data products from the Two Micron All Sky Survey, which is a joint project of the University of Massachusetts and the Infrared Processing and Analysis Center/California Institute of Technology, funded by the National Aeronautics and Space Administration and the National Science Foundation. This study also made use of the VizieR database of astronomical catalogues (Ochsenbein et al. 2000) as well as the NASA/IPAC Extragalactic Database (NED) which is operated by the Jet Propulsion Laboratory, California Institute of Technology, under contract with the National Aeronautics and Space Administration. This research has also made use of data obtained from the Chandra Data Archive and the Chandra Source Catalog, and software provided by the Chandra X-ray Center (CXC) in the application packages CIAO, ChIPS, and Sherpa.

This work is supported in part by the National Aeronautics and Space Administration through Chandra award number GO7-8111X issued by the Chandra X-ray Observatory Center, which is operated by the Smithsonian Astrophysical Observatory for and on behalf of the National Aeronautics and Space Administration under contract NAS8-03060.

REFERENCES

- Assef, R. J., Kochanek, C. S., Brodwin, M., Cool, R., Forman, W., Gonzalez, A. H., Hickox, R. C., Jones, C., Le Floc’h, E., Moustakas, J., Murray, S. S., & Stern, D. 2010, *ApJ*, 713, 970
- Baes, M., Buyle, P., Hau, G. K. T., & Dejonghe, H. 2003, *MNRAS*, 341, L44
- Bentz, M. C., Peterson, B. M., Netzer, H., Pogge, R. W., & Vestergaard, M. 2009, *ApJ*, in press (astro-ph/0812.2283)
- Blandford, R. D., & McKee, C. F. 1982, *ApJ*, 255, 419

- Brand, K., Dey, A., Brown, M. J. I., Watson, C. R., Jannuzi, B. T., Najita, J. R., Kochanek, C. S., Shields, J. C., Fazio, G. G., Forman, W. R., Green, P. J., Jones, C. J., Kenter, A. T., McNamara, B. R., Murray, S. S., Rieke, M., & Vikhlinin, A. 2005, *ApJ*, 626, 723
- Calzetti, D., Wu, S., Hong, S., Kennicutt, R. C., Lee, J. C., Dale, D. A., Engelbracht, C. W., van Zee, L., Draine, B. T., Hao, C., Gordon, K. D., Moustakas, J., Murphy, E. J., Regan, M., Begum, A., Block, M., Dalcanton, J., Funes, J., Gil de Paz, A., Johnson, B., Sakai, S., Skillman, E., Walter, F., Weisz, D., Williams, B., & Wu, Y. 2010, *ApJ*, 714, 1256
- Dale, D. A., Gil de Paz, A., Gordon, K. D., Hanson, H. M., Armus, L., Bendo, G. J., Bianchi, L., Block, M., Boissier, S., Boselli, A., Buckalew, B. A., Buat, V., Burgarella, D., Calzetti, D., Cannon, J. M., Engelbracht, C. W., Helou, G., Hollenbach, D. J., Jarrett, T. H., Kennicutt, R. C., Leitherer, C., Li, A., Madore, B. F., Martin, D. C., Meyer, M. J., Murphy, E. J., Regan, M. W., Roussel, H., Smith, J. D. T., Sosey, M. L., Thilker, D. A., & Walter, F. 2007, *ApJ*, 655, 863
- de Vaucouleurs, G., de Vaucouleurs, A., Corwin, Jr., H. G., Buta, R. J., Paturel, G., & Fouqué, P. 1991, *Third Reference Catalogue of Bright Galaxies. Volume I: Explanations and references. Volume II: Data for galaxies between 0^h and 12^h. Volume III: Data for galaxies between 12^h and 24^h.*, ed. de Vaucouleurs, G., de Vaucouleurs, A., Corwin, H. G., Jr., Buta, R. J., Paturel, G., & Fouqué, P.
- Desroches, L., & Ho, L. C. 2009, *ApJ*, 690, 267
- Eracleous, M., Shields, J. C., Chartas, G., & Moran, E. C. 2002, *ApJ*, 565, 108
- Ferrarese, L. 2002, 3
- Ferrarese, L., & Ford, H. 2005, *Space Science Reviews*, 116, 523
- Filho, M. E., Fraternali, F., Markoff, S., Nagar, N. M., Barthel, P. D., Ho, L. C., & Yuan, F. 2004, *A&A*, 418, 429
- Flohic, H. M. L. G., Eracleous, M., Chartas, G., Shields, J. C., & Moran, E. C. 2006, *ApJ*, 647, 140
- Fruscione, A., McDowell, J. C., Allen, G. E., Brickhouse, N. S., Burke, D. J., Davis, J. E., Durham, N., Elvis, M., Galle, E. C., Harris, D. E., Huenemoerder, D. P., Houck, J. C., Ishibashi, B., Karovska, M., Nicastro, F., Noble, M. S., Nowak, M. A., Primini, F. A., Siemiginowska, A., Smith, R. K., & Wise, M. 2006, in *Presented at the Society*

- of Photo-Optical Instrumentation Engineers (SPIE) Conference, Vol. 6270, Society of Photo-Optical Instrumentation Engineers (SPIE) Conference Series
- Gallo, E., Treu, T., Jacob, J., Woo, J., Marshall, P. J., & Antonucci, R. 2008, *ApJ*, 680, 154
- Georgantopoulos, I., Panessa, F., Akylas, A., Zezas, A., Cappi, M., & Comastri, A. 2002, *A&A*, 386, 60
- Ghosh, H. 2009, PhD thesis, The Ohio State University
- Ghosh, H., Mathur, S., Fiore, F., & Ferrarese, L. 2008, *ApJ*, 687, 216
- Ghosh, H., Pogge, R. W., Mathur, S., Martini, P., & Shields, J. C. 2007, *ApJ*, 656, 105
- Ghosh, H. et al. 2010a, *ApJ*, submitted
- . 2010b, *ApJ*, submitted
- Glozzi, M., Satyapal, S., Eracleous, M., Titarchuk, L., & Cheung, C. C. 2009, *ApJ*, 700, 1759
- González-Martín, O., Masegosa, J., Márquez, I., Guainazzi, M., & Jiménez-Bailón, E. 2009, *A&A*, 506, 1107
- Hasinger, G., Miyaji, T., & Schmidt, M. 2005, *A&A*, 441, 417
- Ho, L. C. 2009, *ApJ*, 699, 626
- Ho, L. C., Feigelson, E. D., Townsley, L. K., Sambruna, R. M., Garmire, G. P., Brandt, W. N., Filippenko, A. V., Griffiths, R. E., Ptak, A. F., & Sargent, W. L. W. 2001, *ApJ*, 549, L51
- Ho, L. C., Filippenko, A. V., & Sargent, W. L. W. 1997, *ApJ*, 487, 568
- Holt, S. S., Schlegel, E. M., Hwang, U., & Petre, R. 2003, *ApJ*, 588, 792
- Hughes, J. P., Chugai, N., Chevalier, R., Lundqvist, P., & Schlegel, E. 2007, *ApJ*, 670, 1260
- Irwin, J. A., Sarazin, C. L., & Bregman, J. N. 2002, *ApJ*, 570, 152
- Kaspi, S., Smith, P. S., Netzer, H., Maoz, D., Jannuzi, B. T., & Giveon, U. 2000, *ApJ*, 533, 631

- Kennicutt, Jr., R. C., Armus, L., Bendo, G., Calzetti, D., Dale, D. A., Draine, B. T., Engelbracht, C. W., Gordon, K. D., Grauer, A. D., Helou, G., Hollenbach, D. J., Jarrett, T. H., Kewley, L. J., Leitherer, C., Li, A., Malhotra, S., Regan, M. W., Rieke, G. H., Rieke, M. J., Roussel, H., Smith, J., Thornley, M. D., & Walter, F. 2003, *PASP*, 115, 928
- Kim, D., & Fabbiano, G. 2003, *ApJ*, 586, 826
- Kormendy, J., & Richstone, D. 1995, *ARA&A*, 33, 581
- Laor, A., Fiore, F., Elvis, M., Wilkes, B. J., & McDowell, J. C. 1994, *ApJ*, 435, 611
- Li, J., Wang, Q. D., Li, Z., & Chen, Y. 2009, *ApJ*, 706, 693
- Luo, B., Chen, J., Zhang, Z., Wang, Y., Wang, J., & Xu, H. 2007, *Chinese Journal of Astronomy and Astrophysics*, 7, 335
- Lutz, D., Sturm, E., Tacconi, L. J., Valiante, E., Schweitzer, M., Netzer, H., Maiolino, R., Andreani, P., Shemmer, O., & Veilleux, S. 2008, *ApJ*, 684, 853
- Magorrian, J., et al. 1998, *AJ*, 115, 2285
- Marconi, A., Risaliti, G., Gilli, R., Hunt, L. K., Maiolino, R., & Salvati, M. 2004, *MNRAS*, 351, 169
- Martini, P., Kelson, D. D., Mulchaey, J. S., & Trager, S. C. 2002, *ApJ*, 576, L109
- Menci, N., Fiore, F., Perola, G. C., & Cavaliere, A. 2004, *ApJ*, 606, 58
- Muñoz-Mateos, J. C., Gil de Paz, A., Zamorano, J., Boissier, S., Dale, D. A., Pérez-González, P. G., Gallego, J., Madore, B. F., Bendo, G., Boselli, A., Buat, V., Calzetti, D., Moustakas, J., & Kennicutt, R. C. 2009, *ApJ*, 703, 1569
- Nemmen, R. S., Storchi-Bergmann, T., Yuan, F., Eracleous, M., Terashima, Y., & Wilson, A. S. 2006, *ApJ*, 643, 652
- Netzer, H. 2009a, *MNRAS*, 399, 1907
- . 2009b, *ApJ*, 695, 793
- Ochsenbein, F., Bauer, P., & Marcout, J. 2000, *A&AS*, 143, 23
- Peterson, B. M. 1993, *PASP*, 105, 247

- Peterson, B. M., Bentz, M. C., Desroches, L., Filippenko, A. V., Ho, L. C., Kaspi, S., Laor, A., Maoz, D., Moran, E. C., Pogge, R. W., & Quillen, A. C. 2005, *ApJ*, 632, 799
- Phillips, A. C., Illingworth, G. D., MacKenty, J. W., & Franx, M. 1996, *AJ*, 111, 1566
- Pogge, R. W., & Martini, P. 2002, *ApJ*, 569, 624
- Rasmussen, J., Ponman, T. J., Verdes-Montenegro, L., Yun, M. S., & Borthakur, S. 2008, *MNRAS*, 388, 1245
- Rinn, A. S., Sambruna, R. M., & Gliozzi, M. 2005, *ApJ*, 621, 167
- Roussel, H., Helou, G., Hollenbach, D. J., Draine, B. T., Smith, J. D., Armus, L., Schinnerer, E., Walter, F., Engelbracht, C. W., Thornley, M. D., Kennicutt, R. C., Calzetti, D., Dale, D. A., Murphy, E. J., & Bot, C. 2007, *ApJ*, 669, 959
- Satyapal, S., Dudik, R. P., O’Halloran, B., & Gliozzi, M. 2005, *ApJ*, 633, 86
- Satyapal, S., Sambruna, R. M., & Dudik, R. P. 2004, *A&A*, 414, 825
- Satyapal, S., Vega, D., Heckman, T., O’Halloran, B., & Dudik, R. 2007, *ApJ*, 663, L9
- Schlegel, E. M., & Pannuti, T. G. 2003, *AJ*, 125, 3025
- Shankar, F., Salucci, P., Granato, G. L., De Zotti, G., & Danese, L. 2004, *MNRAS*, 354, 1020
- Shao, L., Lutz, D., Nordon, R., Maiolino, R., Alexander, D. M., Altieri, B., Andreani, P., Aussel, H., Bauer, F. E., Berta, S., Bongiovanni, A., Brandt, W. N., Brusa, M., Cava, A., Cepa, J., Cimatti, A., Daddi, E., Dominguez-Sanchez, H., Elbaz, D., Förster Schreiber, N. M., Geis, N., Genzel, R., Grazian, A., Gruppioni, C., Magdis, G., Magnelli, B., Mainieri, V., Pérez García, A. M., Poglitsch, A., Popesso, P., Pozzi, F., Riguccini, L., Rodighiero, G., Rovilos, E., Saintonge, A., Salvato, M., Sanchez Portal, M., Santini, P., Sturm, E., Tacconi, L. J., Valtchanov, I., Wetzstein, M., & Wieprecht, E. 2010, *A&A*, 518, L26+
- Shields, J. C., Walcher, C. J., Böker, T., Ho, L. C., Rix, H., & van der Marel, R. P. 2008, *ApJ*, 682, 104
- Skrutskie, M. F., Cutri, R. M., Stiening, R., Weinberg, M. D., Schneider, S., Carpenter, J. M., Beichman, C., Capps, R., Chester, T., Elias, J., Huchra, J., Liebert, J., Lonsdale, C., Monet, D. G., Price, S., Seitzer, P., Jarrett, T., Kirkpatrick, J. D., Gizis, J. E., Howard, E., Evans, T., Fowler, J., Fullmer, L., Hurt, R., Light, R., Kopan, E. L.,

- Marsh, K. A., McCallon, H. L., Tam, R., Van Dyk, S., & Wheelock, S. 2006, *AJ*, 131, 1163
- Strickland, D. K., Heckman, T. M., Colbert, E. J. M., Hoopes, C. G., & Weaver, K. A. 2004, *ApJS*, 151, 193
- Swartz, D. A., Ghosh, K. K., McCollough, M. L., Pannuti, T. G., Tennant, A. F., & Wu, K. 2003, *ApJS*, 144, 213
- Swartz, D. A., Yukita, M., Tennant, A. F., Soria, R., & Ghosh, K. K. 2006, *ApJ*, 647, 1030
- Terashima, Y., & Wilson, A. S. 2001, *ApJ*, 560, 139
- . 2003, *ApJ*, 583, 145
- . 2004, *ApJ*, 601, 735
- Véron-Cetty, M., & Véron, P. 2006, *A&A*, 455, 773
- Veron-Cetty, M. P., & Veron, P. 2010, *VizieR Online Data Catalog*, 7258, 0
- Wandel, A., Peterson, B. M., & Malkan, M. A. 1999, *ApJ*, 526, 579
- White, R. L., Becker, R. H., Helfand, D. J., & Gregg, M. D. 1997, *ApJ*, 475, 479
- Xu, Y., Xu, H., Zhang, Z., Kundu, A., Wang, Y., & Wu, X. 2005, *ApJ*, 631, 809
- Zhang, W. M., Soria, R., Zhang, S. N., Swartz, D. A., & Liu, J. F. 2009, *ApJ*, 699, 281

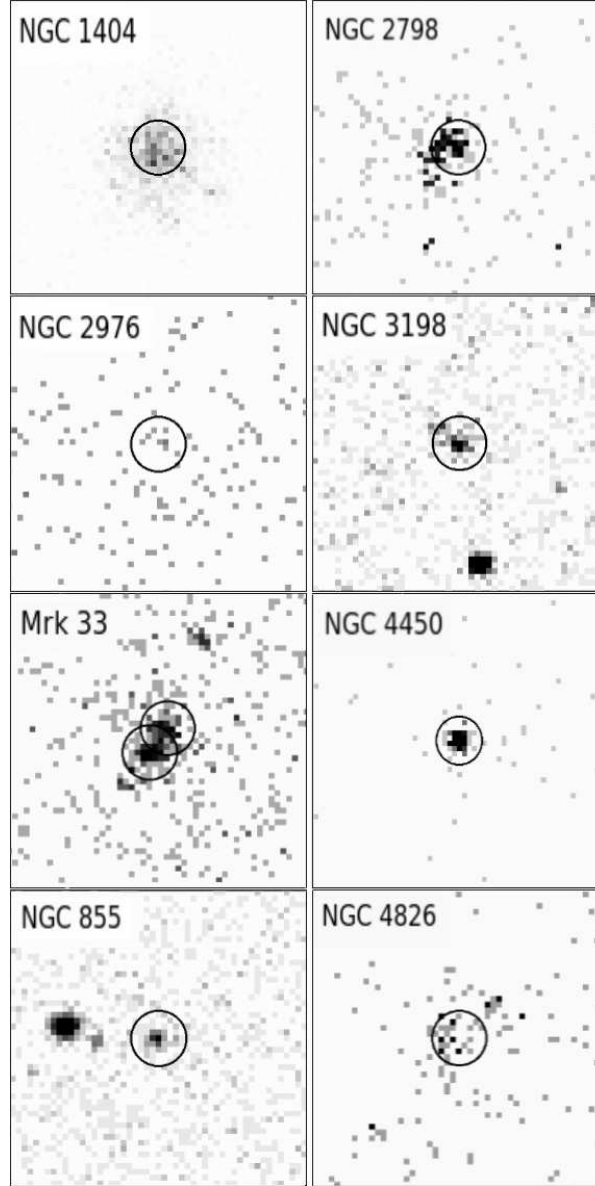


Fig. 1.— Broad band (0.3-8 keV) *Chandra* images for the eight sources with new X-ray detections. Each image is $25'' \times 25''$ in size.

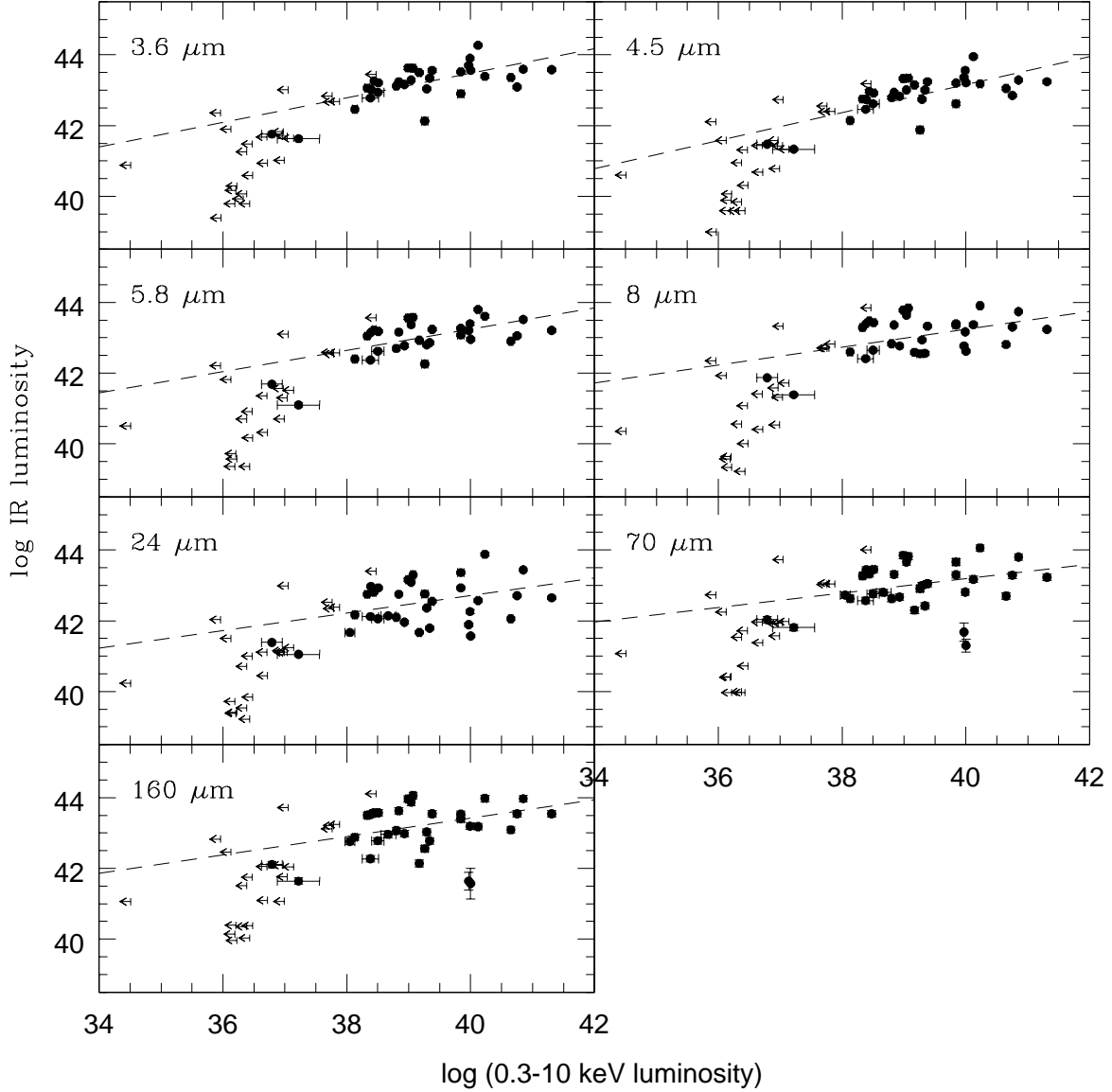


Fig. 2.— *Spitzer* IRAC and MIPS Luminosities of galaxies vs. Nuclear (i.e. AGN) X-ray Luminosity. The dashed line represents the best fit line to the data. Filled circles represent objects in which we have detected the nuclear X-ray source; arrows represent upper limits for those objects whose nuclei were not detected in X-rays.

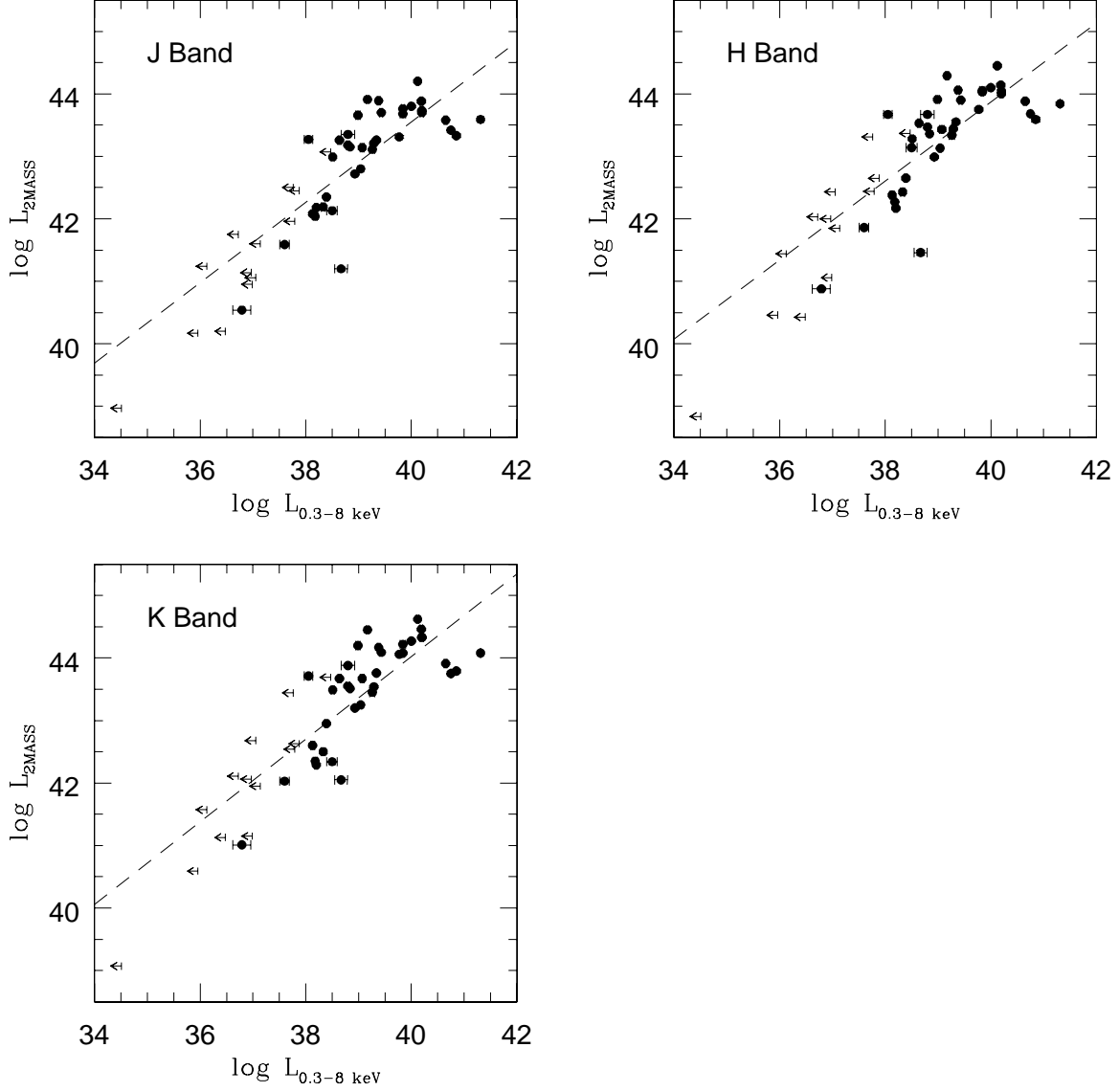


Fig. 3.— Nuclear 2MASS Luminosities vs. Nuclear X-ray Luminosity. The dashed line represents the best fit line to the data. Filled circles represent objects in which we have detected the nuclear X-ray source; arrows represent upper limits for those objects whose nuclei were not detected.

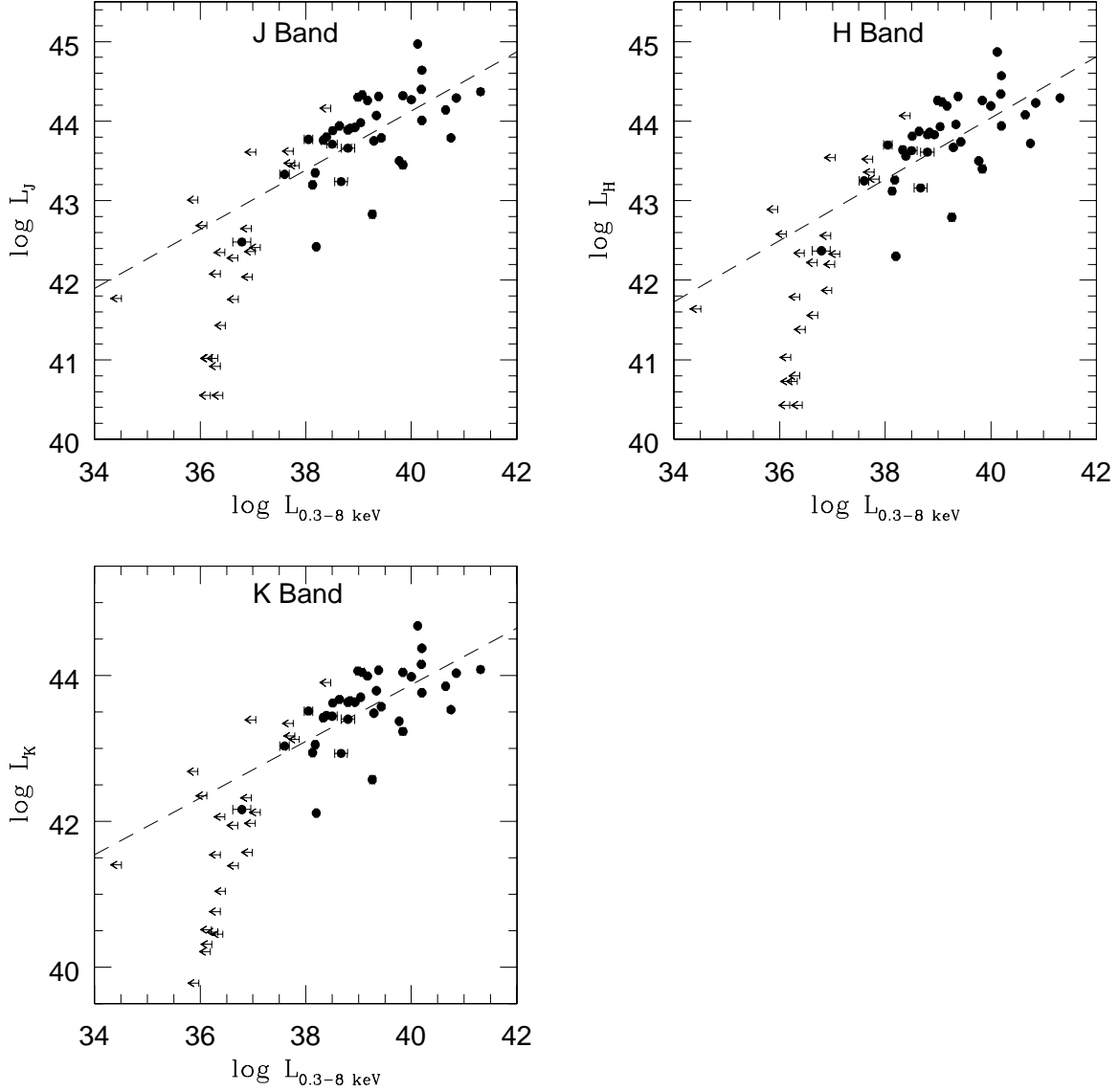


Fig. 4.— Global 2MASS luminosities (from Dale et al. 2007) vs. Nuclear (i.e. AGN) X-ray Luminosity. The dashed line represents the best fit line to the data. Filled circles represent objects in which we have detected the nuclear X-ray source; arrows represent upper limits for those objects whose nuclei were not detected in X-rays.

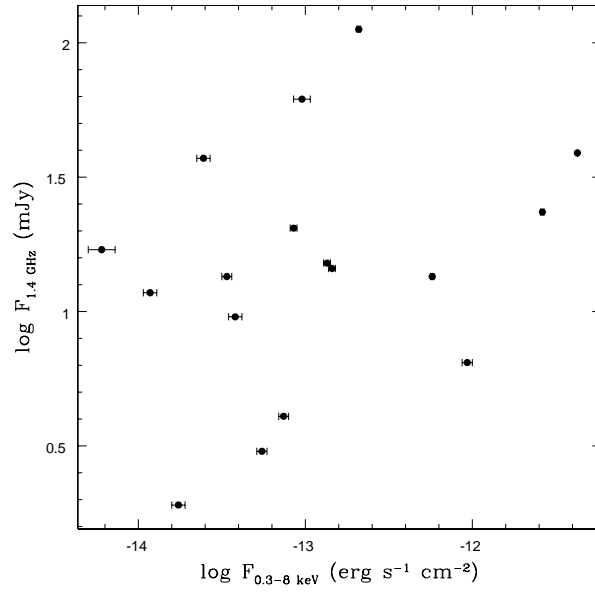


Fig. 5.— Nuclear NVSS & FIRST 1.4 GHz Integrated Flux densities vs. Nuclear X-ray Flux

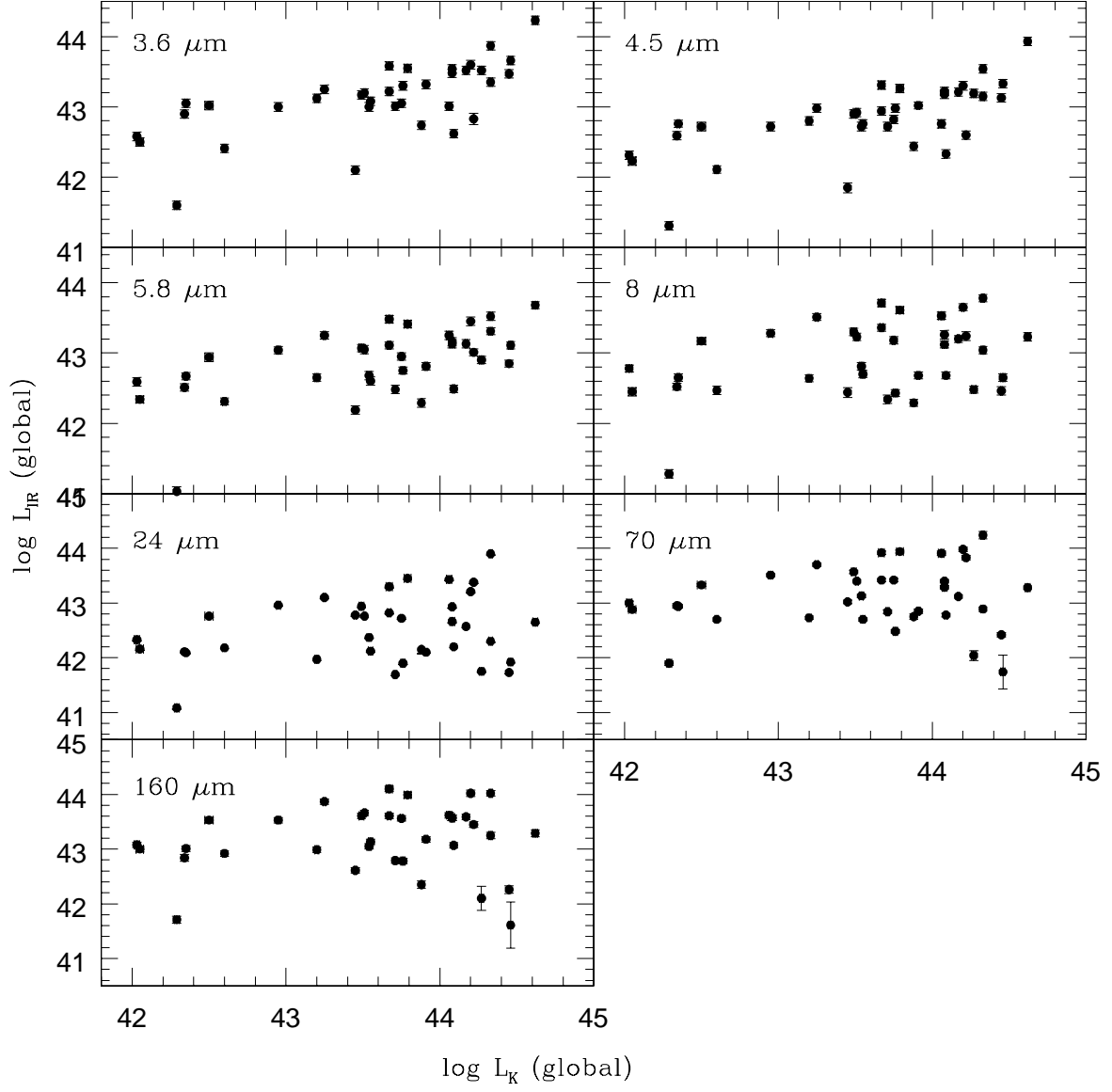


Fig. 6.— Global *Spitzer* IRAC and MIPS Luminosities vs. Global 2MASS K-Band Luminosities (from Dale et al. 2007).

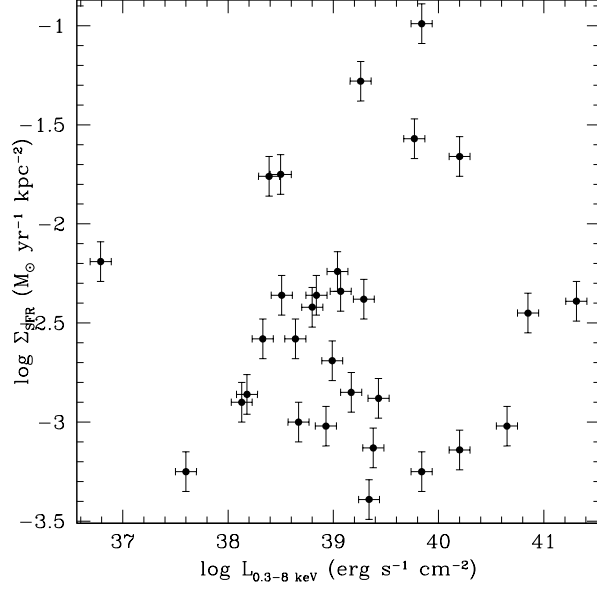


Fig. 7.— Star formation rate per unit area from Calzetti et al. (2010). These were measured using the $24\mu\text{m}$ luminosity and $\text{H}\alpha$ luminosity as SFR indicators and are plotted against the nuclear X-ray flux measured in this work.

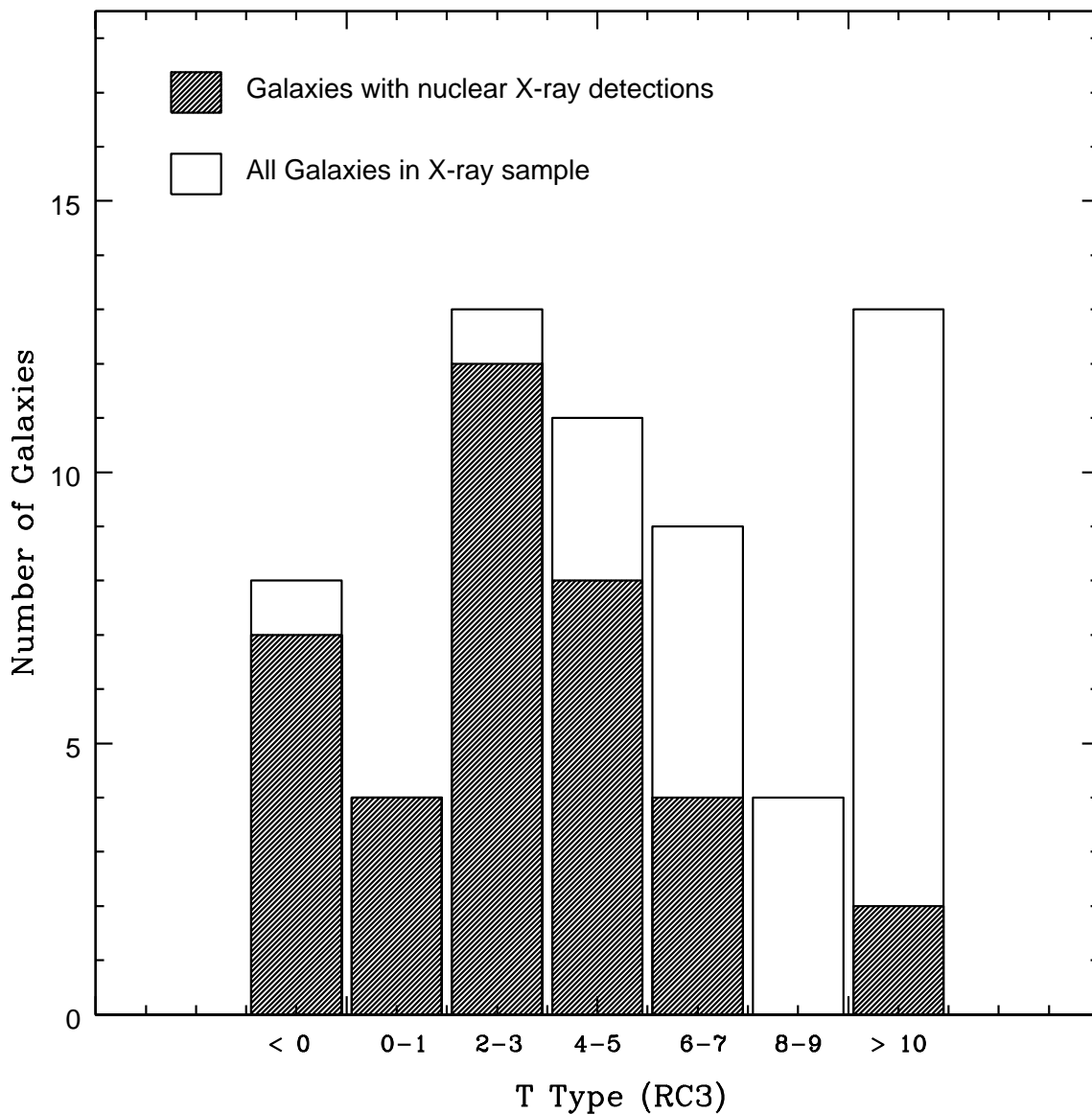


Fig. 8.— Number of galaxies vs. Hubble (T) type. The shaded histogram represents objects in which we have detected the nucleus; the unshaded histogram represents all of the galaxies in the sample. Negative T types represent elliptical and S0 galaxies; $T = 0$ and 1 represent S0/a and Sa galaxies; $T = 2$ and 3 are Sab and Sb, $T = 4$ and 5 are Sbc and Sc galaxies, $T = 6$ and 7 are Scd and Sd galaxies; $T = 8$ and 9 are Sdm and Sm galaxies, and $T \geq 10$ are irregulars and peculiars.

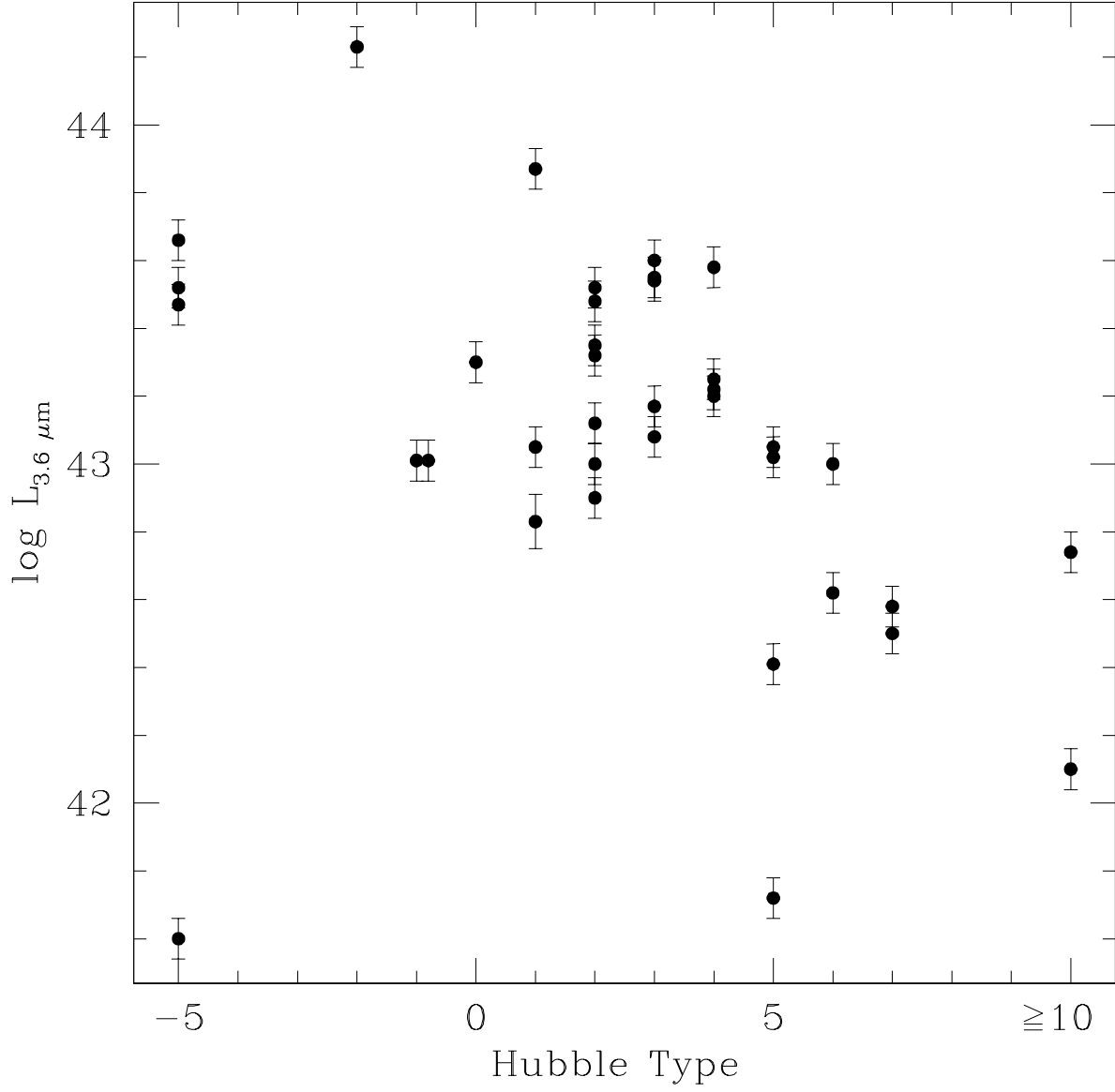


Fig. 9.— Global $3.6\mu\text{m}$ luminosity vs. Hubble Type. Corresponding morphological types are listed in Figure 8.

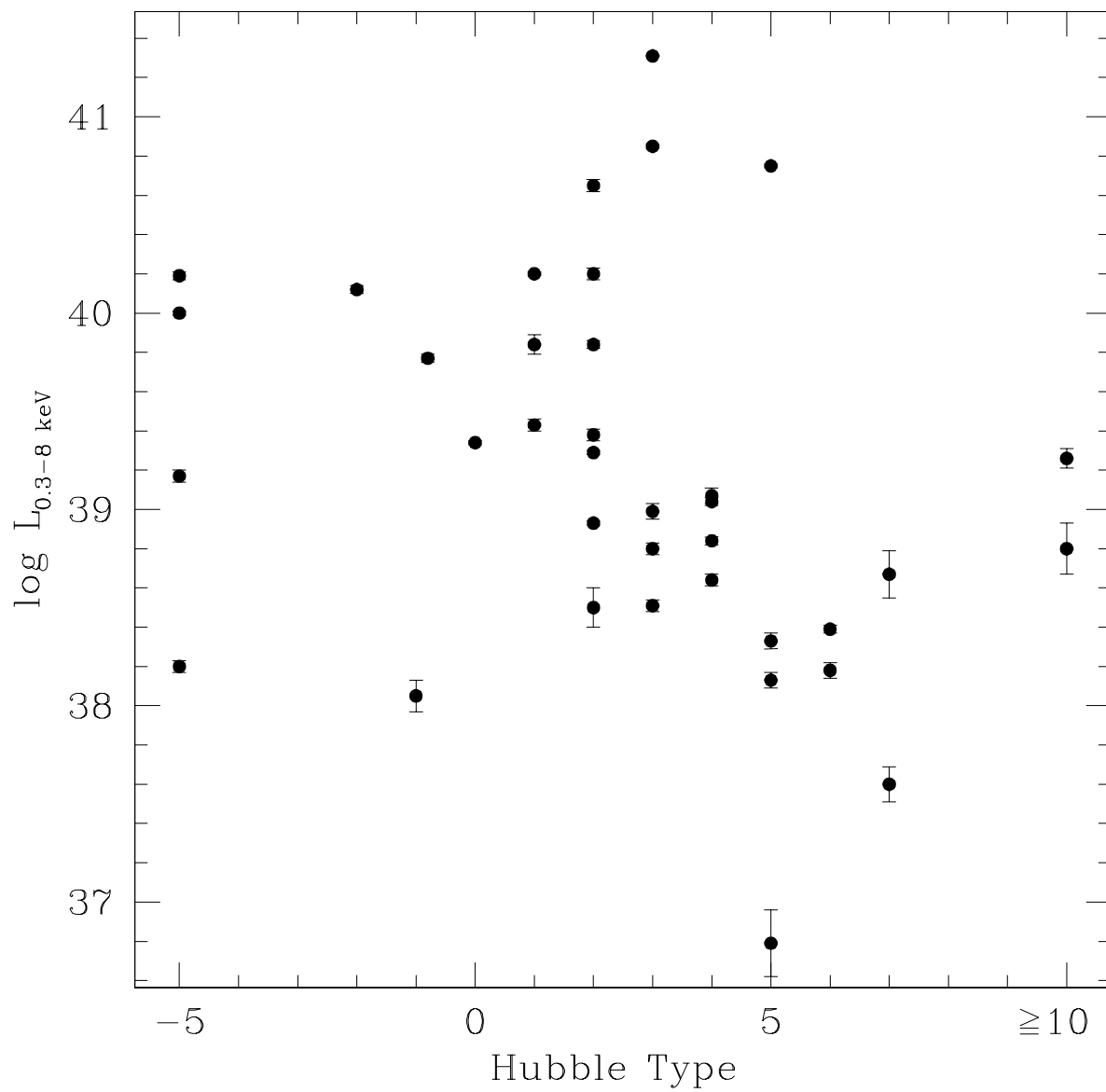


Fig. 10.— Nuclear (AGN) X-ray Luminosity vs. Hubble Type. Corresponding morphological types are listed in Figure 8.

Table 1. SINGS Galaxy Properties and References

Galaxy	RA (J2000)	DEC (J2000)	Morphological Type (RC3)	T (RC3)	Nuclear Type ^a	Dist (Mpc) ^b	R mag ^b	Publications ^c
NGC 0024	00 09 56.5	24 57 47	SAC	5	...	8.2	18.4	1
NGC 0337	00 59 50.1	07 34 41	SBd	7	...	25	20.3	...
NGC 0584	01 31 20.7	06 52 05	E4	-5	...	28	22.2	...
NGC 0628	01 36 41.8	+15 47 00	SAC	5	...	11	20.9	2,3, 4
NGC 0855	02 14 03.6	+27 52 38	E	-5	...	9.6	17.7	2
NGC 0925	02 27 16.9	+33 34 45	SABd	7	H	10.1	20.6	2,5
NGC 1097	02 46 19.0	30 16 30	SBb	3	L	16.9	22.4	6
NGC 1266	03 16 00.7	02 25 38	SB0	-2	Sy	31.3	21.1	...
NGC 1291	03 17 18.6	41 06 29	SBa	0	...	9.7	22.0	2,4, 7
NGC 1316	03 22 41.7	37 12 30	SAB0	-2	L	26.3	23.5	8, 9
NGC 1377	03 36 39.1	20 54 08	S0	-2	H	24.4	19.6	...
NGC 1404	03 38 51.9	35 35 40	E1	-5	...	25.1	22.9	1
NGC 1482	03 54 38.9	20 30 09	SA0	-0.8	...	22	20.5	10
NGC 1512	04 03 54.3	43 20 56	SBab	1	SB	10.4	19.9	...
NGC 1566	04 20 00.4	54 56 16	SABbc	4	Sy1.5	18	21.9	...
NGC 1705	04 54 13.5	53 21 40	Am	-3	SB	5.8	16.7	2
NGC 2403	07 36 51.4	+65 36 09	SABcd	6	H	3.5	19.7	2,5, 11
Ho II	08 19 05.0	+70 43 12	Im	10	...	3.5	17.1	...
M81 DwA	08 23 55.1	+71 01 56	Im	10	...	3.5		1
DDO 053	08 34 07.2	+66 10 54	Im	10	...	3.5	13.6	1
NGC 2798	09 17 22.9	+41 59 59	SBa	1	SB	24.7	19.6	1
NGC 2841	09 22 02.6	+50 58 35	SAB	3	Sy3	9.8	20.7	12, 13
NGC 2915	09 26 11.5	76 37 35	I0	90	SB	2.7	15.1	1
Ho I	09 40 32.3	+71 10 56	IABm	10	...	3.5	13.2	1
NGC 2976	09 47 15.4	+67 54 59	SAC	5	H	3.5	17.6	1
NGC 3049	09 54 49.5	+09 16 16	SBab	2	SB	19.6	18.7	...
NGC 3031 (M81)	09 55 33.2	+69 03 55	SAab	2	L	3.5	21.2	2,13, 14
NGC 3034 (M82)	09 55 52.7	+69 40 46	IO	90	SB	3.5	17.9	2
Ho IX	09 57 32.0	+69 02 45	Im	10	...	3.5	13.6	2
M81 DwB	10 05 30.6	+70 21 52	Im	10	...	3.5	12.5	1
NGC 3190	10 18 05.6	+21 49 55	SAap	1	L	17.4	20.7	15, 16
NGC 3184	10 18 17.0	+41 25 28	SABcd	6	H	8.6	19.0	2,5, 17
NGC 3198	10 19 54.9	+45 32 59	SBc	5	...	9.8	20.2	1
IC 2574	10 28 23.5	+68 24 44	SABm	9	...	3.5	17.7	2
NGC 3265	10 31 06.8	+28 47 48	E	-5	...	20	17.7	...
Mrk 33	10 32 31.9	+54 24 04	Im	10	SB	21.7	18.4	1
NGC 3351	10 43 57.7	+11 42 14	SBb	3	SB	9.3	20.4	2,18
NGC 3521	11 05 48.6	00 02 09	SABbc	4	L	9	21.0	2
NGC 3621	11 18 16.5	-32 48 51	Sad	7	Sy2	6.2	19.4	19
NGC 3627	11 20 15.0	+12 59 30	SABb	3	Sy3	8.9	20.8	2,13
NGC 3773	11 38 12.9	+12 06 43	SA0	-2	...	12.9	17.5	...
NGC 3938	11 52 49.4	+44 07 15	SAC	5	...	12.2	20.1	1
NGC 4125	12 08 06.0	+65 10 27	E6p	-5	...	21.4	21.6	11,20, 21
NGC 4236	12 16 42.1	+69 27 45	SBdm	8	...	3.5	18.1	1

Table 1—Continued

Galaxy	RA (J2000)	DEC (J2000)	Morphological Type (RC3)	T (RC3)	Nuclear Type ^a	Dist (Mpc) ^b	R mag ^b	Publications ^c
NGC 4254	12 18 49.6	+14 24 59	SAC	5	...	20	21.6	4
NGC 4321	12 22 54.9	+15 49 21	SABbc	4	L	20	22.1	2,12, 13
NGC 4450	12 28 29.6	+17 05 06	SAab	2	L	20	21.4	3
NGC 4536	12 34 27.0	+02 11 17	SABbc	4	H	25	20.8	...
NGC 4552	12 35 39.8	+12 33 23	E0	-5	Sy2	20	20.8	20, 22, 23, 3, 12,24,25
NGC 4559	12 35 57.7	+27 57 35	SABcd	6	H	11.6	21.0	2,5
NGC 4569	12 36 49.8	+13 09 46	SABab	2	Sy	20	22.0	13, 21
NGC 4579	12 37 43.5	+11 49 05	SABb	3	L	20	21.8	13, 21, 12,26
NGC 4594	12 39 59.4	11 37 23	SAa	1	Sy3	13.7	21.5	2, 12, 13
NGC 4625	12 41 52.7	+41 16 26	SABmp	9	Sy	9.5	17.5	2,5
NGC 4631	12 42 08.0	+32 32 29	SBd	7	...	9	20.6	2,5
NGC 4725	12 50 26.6	+25 30 03	SABab	2	Sy2	17.1	22.0	2,13
NGC 4736	12 50 53.0	+41 07 14	SAab	2	Sy	5.3	19.9	2,12,24,26
DDO 154	12 54 05.2	+27 08 59	IBm	10	...	5.4	15.1	1
NGC 4826	12 56 43.7	+21 40 58	SAab	2	Sy2	5.6	20.3	2,13
DDO 165	13 06 24.8	+67 42 25	Im	10	...	3.5	15.3	1
NGC 5033	13 13 27.5	+36 35 38	SAC	5	Sy2	13.3	20.9	13,27
NGC 5055	13 15 49.3	+42 01 45	SAbc	4	H/L	8.2	19.0	20,2,12,28
NGC 5194 (M51)	13 29 52.7	+47 11 43	SABbc	4	Sy2	8.2	21.4	2,12,29,21
NGC 5195	13 29 59.6	+47 15 58	SB0p	90	L	8.2	20.0	30,13,21,2,31
NGC 5398	14 01 21.5	33 03 50	SBdm	8.1	H	15	18.9	...
NGC 5408	14 03 20.9	41 22 40	IBm	90	...	4.5	16.1	1
NGC 5474	14 05 01.6	+53 39 44	SACd	6	H	6.9	18.4	2, 5
NGC 5713	14 40 11.5	00 17 20	SABbc	4	...	26.6	20.9	...
NGC 5866 (M102)	15 06 29.5	+55 45 48	SA0	-1	Sy	12.5	19.9	12, 20, 24, 32, 27
IC 4710	18 28 38.0	66 58 56	SBm	9	SB	8.5	18.3	...
NGC 6822	19 44 56.6	14 47 21	IBm	10	...	0.6	13.8	2
NGC 6946	20 34 52.3	+60 09 14	SABcd	6	H	5.5	21.3	5, 2, 33
NGC 7331	22 37 04.1	+34 24 56	SAb	3	L	15.7	21.8	2, 12, 20, 21
NGC 7552	23 16 10.8	42 35 05	SAC	2	H	22.3	21.7	4
NGC 7793	23 57 49.8	32 35 28	SAd	7	H	3.2	18.2	5

^aNuclear identifications: S=Seyfert, SB= starburst, H= nuclear HII region, L= Liner nucleus. Most values are from the RC3 catalog and have been supplemented by values from Veron-Cetty & Veron (2010).

^bFrom Kennicutt et al. (2003)

^cPublications containing analyses of galactic nuclei using *Chandra* data. References: (1) This paper; (2) Zhang et al. 2009; (3) Ho 2009; (4) Ghosh 2009; (5) Desroches & Ho 2009; (6) Nemmen et al. 2006; (7) Irwin et al. 2002; (8) Kim & Fabbiano 2003; (9) Rinn et al. 2005; (10) Strickland et al. 2004; (11) Schlegel & Pannuti 2003; (12) González-Martín et al. 2009 (13) Ho et al. 2001; (14) Swartz et al. 2003; (15) Hughes et al. 2007; (16) Rasmussen et al. 2008; (17) Ghosh et al. 2008; (18) Swartz et al. 2006; (19) Gliozzi et al. 2009; (20) Flohic et al. 2006; (21) Satyapal et al. 2004; (22) Gallo et al. 2008; (23) Xu et al. 2005; (24) Satyapal et al. 2005; (25) Filho et al. 2004; (26) Eracleous et al. 2002; (27) Terashima & Wilson 2003; (28) Luo et al. 2007; (29) Terashima & Wilson 2001; (30) Georgantopoulos et al. 2002; (31) Terashima & Wilson 2004; (32) Li et al. 2009; (33) Holt et al. 2003.

Table 2. Source Information for Nuclear Detections

Object	OBSID	Observation Date	Exposure Time (ks)	CCD	Source RA	Source DEC	Bkg/Src Ratio ^a	Broad Source	Broad Bkg	Net Broad	Net Hard	Net Soft	Hardness Ratio
NGC 0024	9547	13. October 2008	43.22	7	19.60	...	42	< 7	< 6	< 4	...
NGC 0628	2057	19. June 2001	43.2	7	01:36:41.74	15:47:01.19	19.73	97	42	95	22	73	-0.529
NGC 0855	9550	3. October 2008	58.73	7	02:14:03.50	27:52:38.40	18.92	108	98	103	33	69	-0.349
NGC 0925	7104	23. November 2005	2.24	7	02:27:16.87	33:34:45.30	20.91	13	4	13	0	13	...
NGC 1097*	2339	28. January 2001	4	7	02:46:18.97	-30:16:28.98	20.21	1263	382	1244	209	1035	-0.663
NGC 1291*	795	18. July 2001	37.27	7	03:17:18.59	-41:06:28.72	17.40	1102	430	1077	421	656	-0.218
NGC 1316	2022	17. April 2001	25.85	7	03:22:41.69	-37:12:28.71	16.81	702	1483	614	57	557	-0.814
NGC 1404	4174	28. May 2003	43.46	3	03:38:51.93	-35:35:39.06	19.79	938	2782	797	38	759	-0.904
NGC 1482	2932	5. February 2002	24.72	7	03:54:39.32	-20:30:09.53	19.66	417	899	372	172	200	-0.077
NGC 1705	3930	12. September 2003	45.31	7	20.94	...	76	< 9	< 4	< 8	...
NGC 2403	4628	23. August 2004	46.21	7	20.94	...	42	< 4	< 2	< 3	...
M81 DwA	9535	24. August 2008	25.92	7	20.94	...	14	< 2	< 2	< 2	...
DDO 053	9538	3. February 2008	19.02	7	20.94	...	21	< 3	< 2	< 2	...
NGC 2798	10567	24. January 2009	5.11	7	09:17:22.74	42:00:00.12	21.00	76	64	73	7	66	-0.82
NGC 2841	6096	18. December 2004	26.95	7	09:22:02.68	50:58:35.78	19.75	230	193	220	36	184	-0.672
NGC 2915	9534	10. April 2008	15.36	7	20.94	...	17	< 8	< 5	< 6	...
Ho I	9539	22. June 2008	25.92	7	20.94	...	21	< 4	< 2	< 4	...
NGC 2976	9542	24. March 2008	9.82	7	09:47:15.35	67:55:00.10	21.00	7	17	6	5	1	...
NGC 3031*	735	7. May 2000	49.07	7	09:55:33.37	69:03:53.49	20.94	4349	4421	4099	1413	2686	-0.311
NGC 3034 *	8190	2. June 2007	48.99	7	14.20	...	13967	< 138	< 71	< 118	...
Ho IX	9540	24. August 2008	25.72	7	20.94	...	32	< 6	< 3	< 5	...
M81 DwB	9536	7. July 2008	24.93	7	20.60	...	24	< 7	< 4	< 6	...
NGC 3190*	2760	14. March 2002	19.81	7	10:18:05.63	21:49:56.39	21.00	225	98	220	75	145	-0.317
NGC 3184	804	8. January 2000	37.38	7	10:18:16.85	41:25:26.06	19.99	99	61	96	8	88	-0.837
NGC 3198	9551	5. February 2008	61.63	7	10:19:54.95	45:32:58.68	19.24	112	73	108	25	83	-0.535
IC 2574*	9541	30. June 2008	10.78	3	20.94	...	6	< 2	< 1	< 1	...
Mrk 33	9519	1. February 2008	18.25	7	10:32:32.01	54:24:02.16	22.40	103	70	100	18	82	-0.640
NGC 3351*	5931	1. July 2005	39.55	7	17.67	...	572	< 33	< 6	< 32	...
NGC 3521*	9552	28. January 2008	69.69	3	11:05:48.51	-00:02:09.50	16.64	302	159	292	74	218	-0.492
NGC 3621	9278	6. March 2008	19.45	7	11:18:16.50	-32:48:50.59	20.00	23	39	21	3	19	-0.76
NGC 3627	9548	3. November 1999	49.54	7	11:20:15.00	12:59:30.40	15.95	266	234	251	57	195	-0.549
NGC 3938	7862	16. October 2008	4.89	7	19.82	...	21	< 3	< 2	< 2	...
NGC 4125	2071	9. September 2001	62.97	7	12:08:05.95	65:10:27.45	16.86	310	920	255	20	235	-0.841

Table 2—Continued

Object	OBSID	Observation Date	Exposure Time (ks)	CCD	Source RA	Source DEC	Bkg/Src Ratio ^a	Broad Source	Broad Bkg	Net Broad	Net Hard	Net Soft	Hardness Ratio
NGC 4236	9543	20. February 2008	10.87	3	20.89	...	9	< 2	< 2	< 1	...
NGC 4254	7863	21. November 2007	5.07	7	18.47	...	30	< 5	< 2	< 4	...
NGC 4321*	6727	18. February 2006	37.55	7	12:22:54.98	15:49:20.18	19.83	168	629	136	7	129	-0.898
NGC 4450	3997	30. April 2003	1.59	7	12:28:29.59	17:05:05.81	21.00	223	12	222	34	188	-0.695
NGC 4552	2072	22. April 2001	53.79	7	12:35:39.81	12:33:23.05	18.68	1856	3372	1675	157	1518	-0.812
NGC 4559*	2027	4. June 2001	8.87	7	20.94	...	38	< 5	< 2	< 5	...
NGC 4569	5911	13. November 2005	31.29	7	12:36:49.81	13:09:46.09	20.45	681	259	668	84	584	-0.748
NGC 4579	807	2. May 2000	29.95	7	12:37:43.52	11:49:05.61	18.62	19026	1637	18938	4316	14622	-0.544
NGC 4594*	9533	2. December 2008	79.74	3	12:39:59.47	-11:37:22.13	13.34	5154	454	5120	1460	3660	-0.430
NGC 4625	9549	5. March 2008	54.85	7	18.87	...	76	< 10	< 7	< 8	...
NGC 4631	797	16. April 2000	57.32	7	19.30	...	97	< 10	< 7	< 7	...
NGC 4725*	2976	2. December 2002	24.64	7	12:50:26.59	25:30:02.82	21.00	257	114	252	7	244	-0.941
NGC 4736*	808	13. May 2000	43.72	7	12:50:53.07	41:07:12.99	14.03	3851	1354	3754	428	3327	-0.772
DDO 154	9544	3. April 2008	59.2	7	20.94	...	64	< 6	< 4	< 5	...
NGC 4826	411	27. March 2000	1.8	7	12:56:43.60	21:40:57.98	20.62	22	38	20	0	20	...
DDO 165	9537	8. February 2009	0	7	20.94	...	12	< 2	< 1	< 2	...
NGC 5033	412	28. April 2000	2.9	7	13:13:27.47	36:35:38.15	21.00	1148	74	1144	346	799	-0.396
NGC 5055	2197	27. August 2001	28	7	13:15:49.28	42:01:45.77	18.70	370	252	357	78	278	-0.562
NGC 5194*	3932	7. August 2003	41.02	7	13:29:52.71	47:11:42.98	17.17	915	1462	830	76	754	-0.818
NGC 5195	414	23. January 2000	1.14	7	13:29:59.49	47:15:57.86	21.00	12	16	11	2	9	-0.64
NGC 5408*	4558	29. January 2005	4.1	7	20.94	...	14	< 2	< 1	< 2	...
NGC 5474	9546	3. December 2007	29.76	7	20.94	...	37	< 4	< 3	< 3	...
NGC 5866	2879	14. November 2002	30.26	7	15:06:29.58	55:45:48.48	18.51	40	242	27	19	8	0.389
IC 4710*	9570	25. June 2008	30.36	7	20.91	...	34	< 6	< 5	< 3	...
NGC 6822	2925	4. November 2002	20.21	3	21.25	...	5	< 1	< 1	< 0	...
NGC 6946*	1043	7. September 2001	58.29	7	20:34:52.31	60:09:14.39	18.77	549	239	536	100	436	-0.628
NGC 7331	2198	27. January 2001	27.9	7	22:37:04.00	34:24:55.53	17.11	152	291	135	29	106	-0.577
NGC 7552	7848	31. March 2007	5.08	7	23:16:10.66	-42:35:03.64	21.00	207	238	196	13	183	-0.87
NGC 7793	3954	6. September 2003	46.41	7	20.94	...	30	< 8	< 4	< 7	...

^aThe ratio of the area of the background extraction region to the area of the source extraction region.*These galaxies have multiple *Chandra* observations; we present here only the results from the longest and/or most recent data sets.

Table 3. Nuclear Source Fluxes and Luminosities

Object	0.3-8 keV Count rate (10^{-3} counts s^{-1})	0.3-8 keV Flux (10^{-14} erg s^{-1} cm^{-2})	$\log L_{0.3-8keV}$ (erg s^{-1})
NGC 0024	< 2	< 0.12	< 36.97
NGC 0628	22 ± 2	1.48 ± 0.15	38.33 ± 0.04
NGC 0855	18 ± 2	1.18 ± 0.12	38.21 ± 0.03
NGC 0925	57 ± 16	3.85 ± 1.08	38.67 ± 0.12
NGC 1097	3109 ± 88	208.5 ± 5.91	40.85 ± 0.01
NGC 1291	289 ± 9	19.38 ± 0.59	39.34 ± 0.01
NGC 1316	237 ± 10	15.92 ± 0.64	40.12 ± 0.02
NGC 1404	183 ± 6	20.57 ± 0.73	40.19 ± 0.02
NGC 1482	150 ± 8	10.09 ± 0.52	39.77 ± 0.02
NGC 1705	< 2	< 0.13	< 36.72
NGC 2403	< 1	< 0.06	< 35.96
M81 DwA	< 1	< 0.06	< 35.97
DDO 053	< 2	< 0.11	< 36.19
NGC 2798	143 ± 17	9.58 ± 1.12	39.84 ± 0.05
NGC 2841	82 ± 6	5.49 ± 0.37	38.8 ± 0.03
NGC 2915	< 5	< 0.35	< 36.48
Ho I	< 2	< 0.11	< 36.21
NGC 2976	6 ± 3	0.42 ± 0.17	36.79 ± 0.17
NGC 3031	835 ± 13	57.62 ± 0.90	38.93 ± 0.01
NGC 3034	< 28	< 1.89	< 37.44
Ho IX	< 2	< 0.15	< 36.33
M81 DwB	< 3	< 0.18	< 36.43
NGC 3190	111 ± 7	7.46 ± 0.50	39.43 ± 0.03
NGC 3184	26 ± 3	1.73 ± 0.18	38.18 ± 0.04
NGC 3198	18 ± 2	1.18 ± 0.11	38.13 ± 0.04
IC 2574	< 1	< 0.17	< 36.38
Mrk 33	48 ± 5	3.84 ± 0.38	39.26 ± 0.05
NGC 3351	< 8	< 0.55	< 37.76
NGC 3521	42 ± 2	4.56 ± 0.27	38.64 ± 0.03
NGC 3621	11 ± 2	< 0.81 ± 0.18	37.57 ± 0.09
NGC 3627	51 ± 3	3.40 ± 0.21	38.51 ± 0.03
NGC 3938	< 6	< 0.42	< 37.88
NGC 4125	41 ± 3	2.72 ± 0.17	39.17 ± 0.03
NGC 4236	< 2	< 0.20	< 36.47 0
NGC 4254	< 9	< 0.62	< 38.47
NGC 4321	36 ± 3	2.43 ± 0.21	39.07 ± 0.04
NGC 4450	1395 ± 94	93.51 ± 6.27	40.65 ± 0.03
NGC 4552	312 ± 8	20.88 ± 0.51	40 ± 0.01
NGC 4559	< 6	< 0.38	< 37.79
NGC 4569	214 ± 8	14.31 ± 0.55	39.84 ± 0.02
NGC 4579	6323 ± 46	423.80 ± 3.08	41.31 ± 0
NGC 4594	642 ± 9	69.87 ± 0.98	40.2 ± 0.01
NGC 4625	< 2	< 0.13	< 37.14

Table 3—Continued

Object	0.3-8 keV Count rate (10^{-3} counts s $^{-1}$)	0.3-8 keV Flux (10^{-14} erg s $^{-1}$ cm $^{-2}$)	$\log L_{0.3-8\text{keV}}$ (erg s $^{-1}$)
NGC 4631	< 2	< 0.12	< 37.05
NGC 4725	102 ± 6	6.86 ± 0.43	39.38 ± 0.03
NGC 4736	859 ± 14	57.66 ± 0.94	39.29 ± 0.01
DDO 154	< 1	< 0.07	< 36.38
NGC 4826	112 ± 25	8.34 ± 1.86	38.5 ± 0.1
DDO 165	< 2	< 0.11	< 36.22
NGC 5033	3944 ± 117	265.0 ± 7.86	40.75 ± 0.01
NGC 5055	127 ± 7	8.55 ± 0.45	38.84 ± 0.02
NGC 5194	202 ± 7	13.57 ± 0.47	39.04 ± 0.02
NGC 5195	99 ± 29	7.37 ± 2.20	38.38 ± 0.13
NGC 5408	< 6	< 0.40	< 36.99
NGC 5474	< 1	< 0.09	< 36.71
NGC 5866	9 ± 2	0.60 ± 0.11	38.05 ± 0.08
IC 4710	< 2	< 0.13	< 37.04
NGC 6822	< 1	< 0.08	< 34.51
NGC 6946	92 ± 4	6.75 ± 0.29	38.39 ± 0.02
NGC 7331	48 ± 4	3.28 ± 0.28	38.99 ± 0.04
NGC 7552	385 ± 28	28.70 ± 2.05	40.23 ± 0.03
NGC 7793	< 2	< 0.11	< 36.13

Table 4. Fit Parameters for IR/X-Ray Correlations

Wavelength/ Band	$L/L_{0.3-8\text{keV}}$	Intercept	Spearman Coefficient	Pearson Coefficient	$P(r)^a$
3.6 μm	0.365	28.75	0.67	0.65	<0.1%
4.5 μm	0.360	28.68	0.70	0.66	<0.1%
5.8 μm	0.295	31.28	0.61	0.59	<0.1%
8 μm	0.212	34.58	0.36	0.44	$\sim 1\%$
24 μm	0.243	32.94	0.28	0.38	$\sim 10\%$
70 μm	0.218	34.62	0.27	0.27	$\sim 10\%$
160 μm	0.249	33.52	0.27	0.27	$\sim 10\%$
<i>J</i> Band (global)	0.372	29.25	0.64	0.63	<0.1%
<i>H</i> Band (global)	0.386	28.6	0.66	0.64	<0.1%
<i>K</i> Band (global)	0.388	28.35	0.66	0.65	<0.1%
<i>J</i> Band (nuclear)	0.643	17.83	0.77	0.77	<0.1%
<i>H</i> Band (nuclear)	0.632	18.59	0.76	0.76	<0.1%
<i>K</i> Band (nuclear)	0.661	17.58	0.78	0.74	<0.1%

^aProbability that there is in fact no correlation between the two parameters